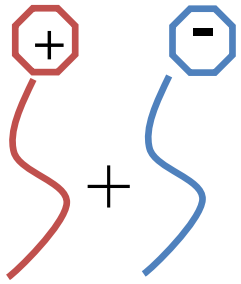

Polyelectrolytes

Chitosan + RSNa

Add CHON dropwise into chitosan solution

Stirred at 1000 rpm for 2 hr

RSNa loaded PECN

Chapter-8

Formulation development of RSNa loaded PECN

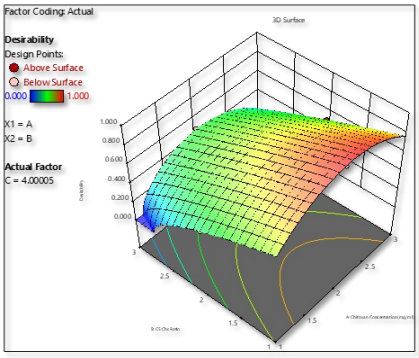

Optimization by BBD

Evaluation of RSNa loaded PECN

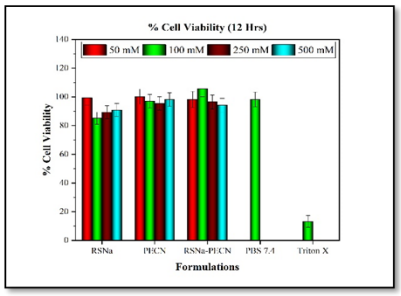

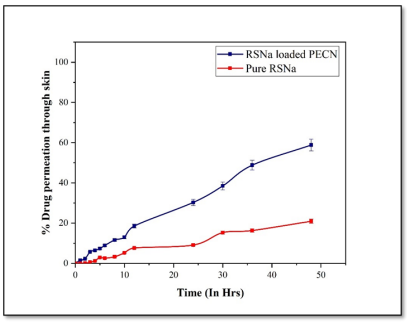

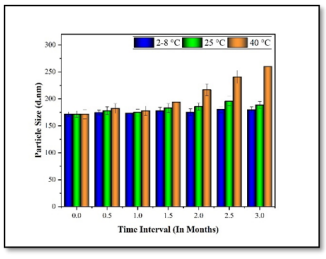

Stability study

8.1. Preparation of RSNa loaded PECN:

The RSNa loaded PECN were prepared by ionic gelation method with some modification [1, 2]. The solution of chitosan was prepared in 1 % acetic acid and its pH was adjusted upto 4 using 1M NaOH. RSNa was dissolved into chitosan solution and stirred for 15 min. The chondroitin sulfate solution was added dropwise into the chitosan solution with continuous stirring at 1000 RPM for 2 hrs at 25°C. The resulting nanoparticle dispersion was centrifuged at 20000 rpm for 20 min (3 cycles) at 20°C to remove unentrapped drug, the supernatant was separated and NPs pellet was resuspended in purified water.

8.2. Selection of polyelectrolytes:

In this present work, we have tried different anionic and cationic polyelectrolytes for preparation of polyelectrolyte complex nanoparticles. The chitosan were tried as cationic polyelectrolytes, while dextran sulfate, hyaluronic acid, pectin, alginate, chondroitin sulfate etc tried as anionic polyelectrolytes for development of PECN. The selection of anionic and cationic polyelectrolyte was done based on higher entrapment efficiency with minimum particle size.

8.3. Optimization:

After selection of polyelectrolytes, the process and formulation variables that could have a significant effect on the % entrapment efficiency and particle size were determined. The different variables for preliminary include speed of stirring, stirring time, rate of addition, pH of chitosan solution, chitosan concentration, chitosan:chondroitin sulfate ratio etc. Among these, Chitosan concentration, chitosan:chondroitin sulfate ratio and pH of chitosan solution showed significant effect on particle size (PS) and % Entrapment efficiency (% EE) and were found to be critical variables. Hence, these parameters were further optimized by Box-Behnken design (response surface methodology).

8.4. Screening and optimization of process and formulation parameters:

The process and formulation variables were optimized by one factor at a time (OFAT) approach. Various process variables such as speed of stirring, stirring time and rate of addition as well as formulaion variables such as pH of chitosan solution, chitosan

concentration, and chitosan:chondroitin sulfate ratio were screened and optimized on the basis of minimum PS and maximum % EE.

8.5. Experimental design:

The three level three factor Box-Behnken design (BBD) was used to optimise the RSNa loaded PECN and create a polynomial model for the optimization process. The experimental design and their statistical analysis were made by DesignExpert Software (version 13, Sate-Ease Inc. Minneapolis, MN, USA). Total 16 experimental runs were obtained from design, from that, 13 batches represent mid-point of each edge of multidimensional cube and the residual three runs are replicates of the cube's centre points. Three independent factors were selected viz. Chitosan concentration, chitosan:chondroitin sulfate ratio and pH of chitosan solution. The particle size and entrapment efficiency were selected as dependent variables. Table- 8.2 represents the independent and dependent variables with their levels and goals respectively.

Table- 8.2. Variables investigated in RSNa loaded PECN using BBD.

Variables	**Levels**	
	Low	**High**
Chitosan concentration (mg/mL)	1	3
CS/CHON ratio	1:1	3:1
pH of chitosan solution	4	6

Responses	**Goal**	**Importance**
Particle Size (d.nm)	Minimum	+++
Entrapment Efficiency (%)	Maximum	+++

The check point batch obtained from the design was prepared to validate and confirm batch-to-batch variability.

8.6. Physicochemical characterization of RSNa loaded PECN:

a. Physicochemical characteristics of RSNa loaded PECN:

The average particle size, polydispersity index and zeta potential of optimized PEC nanoparticles was analysed by Zetasizer nano ZS-90 (Malvern Instruments, Malvern, UK) [3]. The prepared nanoparticles were centrifuged for 20 min at 20000 rpm (3 cycles) at 20°C. The supernatant was analyzed by UV visible spectroscopy. The entrapment efficiency (%) was calculated by following formula [2]:

$$Entrapment\ efficiency\ (\%) = \frac{Total\ RSNa\ added - Unentrapped\ RSNa}{Total\ RSNa\ added} \times 100$$

…… equation- 8.1

The loading capacity (%) of formulation was calculated as follows:

$$Loading\ Capacity\ = \frac{Total\ RSNa\ added - Unentrapped\ RSNa}{Total\ solid\ content} \times 100$$

…… equation- 8.2

The surface morphology of RSNa loaded PECN was analyzed by transmission electron microscope (TEM, Philips Tecnai 20) [2]. Drug and optimized formulation were analyzed by FTIR spectrophotometer (84000S, Shimadzu, Japan) over a range of 4000 to 400 cm^{-1} wavenumber in an inert atmosphere [4, 5]. Differential Scanning Calorimetry analysis of RSNa and RSNa loaded PECN was carried out with Shimadzu DSC-60 (Japan) [6]. The X-ray diffraction analysis was analyzed to check the physical state of different components of the optimized formulation by wide angle X-ray scattering (Philips, PW 1710) with a copper anode using Sc as a detector. It was conducted at room temperature and absolute intensity was observed in the range of 10-50 versus 2θ [7, 8].

8.7. In vitro drug release study:

The drug release profile from RSNa and RSNa loaded PECN was performed by dialysis method (MW cut-off of 12k-14k Da) in 50 ml of saline phosphate buffer pH 7.4 as well as pH 5.5, under magnetic stirring at 100 rpm at 37°C. The samples were withdrawn from diffusion medium at predetermined time intervals upto 48 hrs and replaced with same amount of freshly prepared diffusion medium to maintain sink conditions. The

withdrawn samples were filtered through 0.45 µm syringe filter and analyzed by HPLC method (described in chapter 3).

To describe the release profile, the data was fitted to various exponential equations, including the Zero order, First order, Higuchi, and Korsmeyer-Peppas model [7].

8.8. *Ex vivo* skin permeation study:

Rat skin was mounted on the Franz diffusion cell in such a way that stratum corneum faced the donor receptor and dermis side faced the receptor compartment. The receptor compartment was filled with phosphate buffer 7.4 at 32 ± 0.5°C under constant magnetic stirring at 100 rpm. The pure drug and formulation (RSNa loaded PECN) were placed in donor compartment and samples were withdrawn from receptor medium at predetermined time intervals and replaced with freshly prepared medium. The withdrawn samples were filtered through 0.45 µm syringe filter and analyzed spectrophotometrically [9]. The data was plotted as % cumulative drug permeated through skin as a function of time [10].

After completion of permeation study, the skin was removed from Franz diffusion cell after study completion and the donor side was washed with PBS and collected the washed sample for calculation of drug remained on skin. The skin was then cut into small pieces and suspended into PBS. The suspension was homogenized for 15 min and sonicated using bath sonicator to remove drug which was accumulated into skin layers. After that, the samples were centrifuged for 10 minutes at 5000 rpm. The supernatant was collected and filtered through 0.45 µm syringe filter and analyzed [11-14].

The permeation enhancement ratio (PER) was calculated as follows [10]:

$$PER = \frac{J_{ss}\ Test}{J_{ss}\ Control}$$

…….equation- 8.3.

8.9. In vitro cell line study:

Cell culture:

Skin fibroblast cells (3T3 Swiss albino) and keratinocytes were purchased from NCCS, Pune, India and grown in T-25 cell culture flask incubated in CO_2 incubator in 5% CO_2

and 100% humidity at 37°C. The culture growth media contained DMEM (high glucose), 10% foetal bovine serum, and 1% antibiotic [15, 16].

1. **Cytotoxicity assessment by MTT assay:**

   The skin fibroblast cells-3T3 [17] (7500 cells/well) were seeded in 96-well plates filled with 200 µl of culture growth medium. After 24 hrs, the cells were washed with sterile phosphate buffer 7.4 and replaced with fresh growth medium. Then cells were treated for 12 and 24 hrs with drug solution, placebo formulation and drug loaded PECN at concentration of 50, 100, 250 and 500 µM in triplicates. Untreated cells were used as negative control and triton X-100 treated cells were used as positive control. After completion of treatment period of 12 hrs and 24 hrs, the cells were washed with fresh medium at least three times and MTT reagent (1mg/ml in PBS) was added to each well. After 2-3 hrs, formed formazan crystals were dissolved in 100 µl of dimethyl sulfoxide and their concentration was spectrophotometrically quantified at 570 nm with a microplate reader (680 XR, Bio-rad Laboratories, USA). The results were represented as % of cell viability in comparison with non-treated cells [18, 19].

2. **In vitro cell permeability study:**

   In vitro cell permeability study was performed across fibroblasts and keratinocytes monolayer (apical to basolateral). Transwell® inserts of 12 mm diameter, 0.4 µm pore size (Corning, USA) with surface area of 1.12 cm^2 were used. According to standard protocol for permeability study, fibroblast cells were cultivated on filter support at a density of 4×10^5 cells per well. The cells were maintained by changing media every alternate day for 21 days. The integrity of the monolayers was checked by monitoring the trans-epithelial resistance measurement using Millicell® ERS meter (Millipore, Bedford, Massachusetts, USA). After incubation, transepithelial permeation from apical (AP) to basolateral (BL) was carried out by placing pure drug and their formulations equivalent to 300 µg prepared in growth medium on the AP side, and 2.5 mL of DMEM on the BL side. Samples (200 µL) were withdrawn from BL compartments at predetermined time interval over 12 hrs. Withdrawn samples were stored at -20 °C until analysis by HPLC (as described in in vitro drug

release study). The apparent permeability coefficient (Papp in cm/s) from apical-to-basolateral was calculated as follows:

$$\text{Papp} = \frac{\text{Flux}}{\text{Initial concentration}}$$

…… equation- 8.4

Where, Papp is the apparent permeability co-efficient (cm/s) [20-22].

8.10. Stability study:

The storage stability of drug loaded PECN dispersion was carried out at 2-8 °C, 25 ± 2°C/60 ± 5% RH and 40 ± 2°C/75 ± 5% RH in air tight container for 90 days. Samples were monitored by analysing for average particle size and % assay at interval of 15 days [23, 24].

8.11. Results and discussion:

RSNa loaded PECN: Formulation development

The present works covers the formulation and evaluation of RSNa loaded PECN as well as identification of several critical formulation and process factors that mainly effected PS and % EE. After the identification and selection of essential variables, preliminary study was performed to determine optimal operating ranges, which were then used to optimise each of the parameters using response surface methodology.

8.12. Preliminary screening for RSNa loaded PECN:

Based on trial and error as well as a literature survey, several process and formulation factors that could affect PS and % EE were screened. Among these, important factors with significant effect on quality attributes were selected for preliminary investigation.

8.12.1. Selection of polyelectrolytes:

An important set of criteria for development of PECN was selection of cationic and anionic polyelectrolytes on the basis of lowest particle size and highest entrapment efficiency. Among several polyelectrolytes, the PECN prepared using chitosan as cationic polyelectrolyte and chondroitin sulfate as anionic polyelectrolytes showed minimum PS and maximum % EE (shown in table- 8.3). Thus, chitosan and chondroitin sulfate were selected as polyelectrolytes for preparation of PECN.

Table- 8.3. Selection of polyelectrolytes

Selection of polyelectrolytes			
Polyelectrolytes		**Observation**	
Cationic	**Anionic**	**Particle Size (d.nm)**	**Entrapment efficiency (%)**
Chitosan	Dextran sulfate	282.0 ± 5.29	46.82 ± 2.51
	Hyaluronic acid	363.8 ± 8.63	41.26 ± 1.69
	Chondroitin sulfate	226.2 ± 4.12	56.72 ± 1.14
	Sodium alginate	312.4 ± 7.19	42.51 ± 2.63
	Pectin	294.1 ± 5.36	48.18 ± 1.84

(n=3, ± S.D.)

8.12.2. Risk analysis and mitigation:

After the selection of polyelectrolytes, a risk analysis was conducted for the formulation of RSNa loaded PECN. Risk analysis is nothing but the determination of important factors, the slight change in which can result in decline in product quality. The FishBone diagram (Figure- 8.1) was constructed on the basis of literature review to identify formulation and process variables that might alter the quality of PECN. The quality target or Critical Quality Attributes (CQA) for RSNa loaded PECN was higher entrapment efficiency with smaller particle size, as these factors are connected to the therapeutic efficacy of the prepared PECN. During the preliminary tests, the variables with a low or medium influence on the PECN were optimised using the One Variable At a Time (OVAT) technique, whilst the high-risk factors were taken into consideration (shown in table- 8.4) and optimised using the Box-Behnken design (BBD). Only process and formulation factors were examined for risk analysis in this case, whereas drug substance properties were assumed to be constant because the drug utilised was of the same lot number throughout the study.

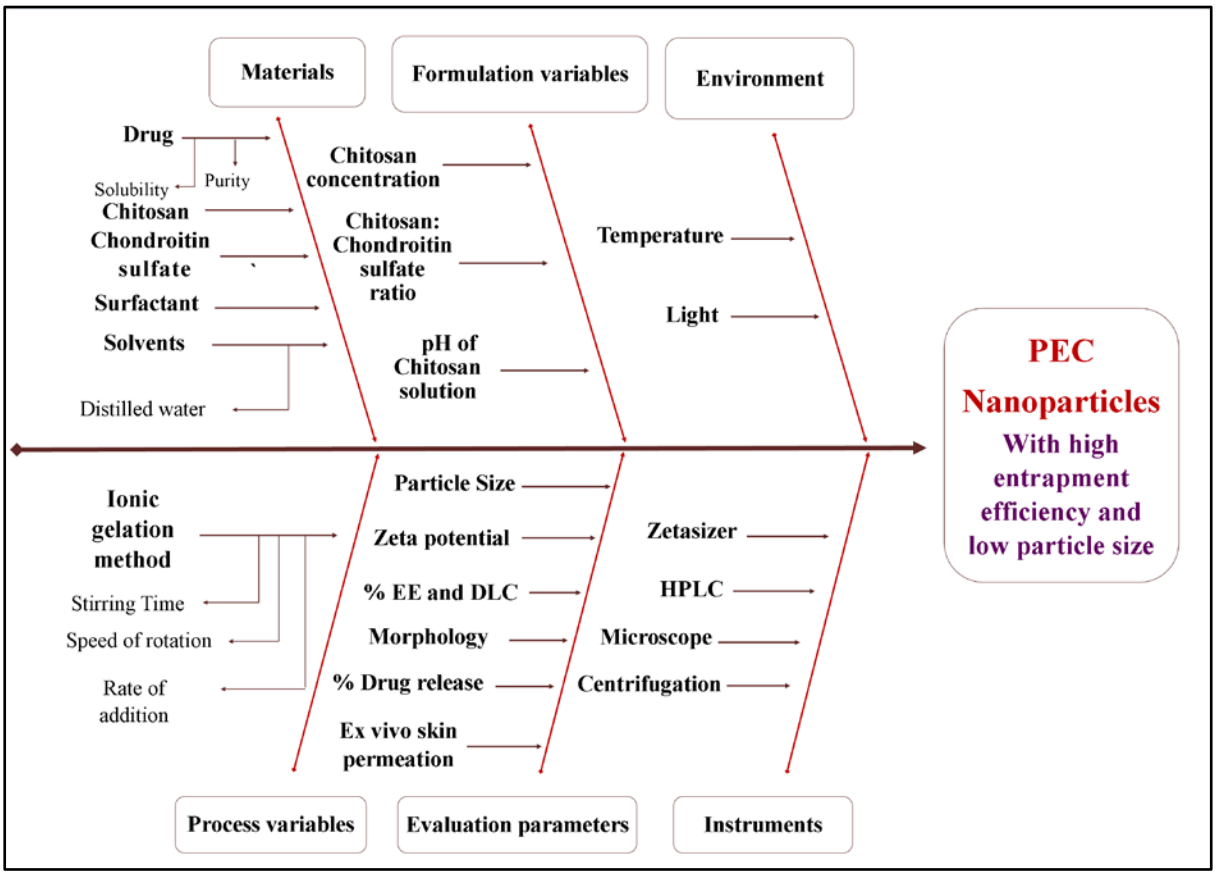

Figure- 8.1. FishBone diagram for selection of variables for development of PECN

Table- 8.4 Risk analysis to identify critical parameters for formulation of RSNa loaded PECN

Critical Quality Attributes (CQA)	Process variables			Formulation Variables		
	Stirring time (Hrs)	Stirring speed (RPM)	Rate of addition (mL/min)	Chitosan concentration (mg/dL)	Chitosan: chondroitin sulfate ratio	pH of chitosan solution
Particle Size (d.nm)	M	M	M	H	H	H
Entrapment efficiency (%)	L	L	L	H	H	H

8.12.3. Screening and optimization of process parameters for preparation of PECN:

The process parameters for preparation of RSNa loaded PECN such as rate of addition, speed of rotation and stirring time were screened on the basis of minimum particle size with maximum entrapment efficiency (shown in table- 8.5) and optimized as follows:

a. Selection of rate of addition:

The results showed that flash addition of solution resulted in formation of larger particles. This might be explained by the higher concentration of CHON at the interface between the chitosan and chondroitin sulfate solution due to rapid mixing process resulted in formation of non-uniform complexes at higher rate of addition [25]. 1.0 mL/min showed smaller particle size and high entrapment efficiency as compared to 0.5 as well as 2.0 mL/min. Thus, 1.0 mL/min rate of addition was selected as optimum for further development.

b. Selection of speed of rotation:

It was observed that increase in speed of rotation decreased PS and increased EE upto 1000 rpm. This happened due to an increase in the shear force, which was the effect of accelerating CHON dispersion in chitosan solution, which led to more cross-linkages in chitosan [25-27]. Beyond 1000 rpm, intense stirring may reduce the repulsive force between particles and lead to the aggregation of the particles [27]. Thus, on the basis of minimum PS and high % EE, 1000 rpm was selected as optimum speed of rotation for further development.

c. Selection of stirring time:

The results of screening and optimization of stirring time showed that 2 hrs of stirring time was sufficient to produce nanoparticles with low PS and high % EE due to the fact that it provided sufficient time to take orientation and prolong the exposure of chitosan to chondroitin sulfate for the formation of PECN [28]. Beyond 2 hrs, PS increased with decrease in %EE. The excessive stirring can also lead to particle aggregation and instability. This is because prolonged stirring can cause shear forces that can break up the nanoparticles or cause them to stick together [29]. Hence, 2 hrs was selected as optimum stirring time for further development.

Table- 8.5. Effect of process parameters on preparation of RSNa loaded PECN

Selection of rate of addition		
Rate of addition	**Observations**	
	PS (d.nm)	**% EE**
Flash addition	551.2 ± 9.68	21.67 ± 1.20
0.5	258.2 ± 5.84	52.88 ± 2.36
1.0	226.2 ± 4.12	56.72 ± 1.14
2.0	359.6 ± 5.36	42.66 ± 2.22
Selection of speed of rotation		
Speed of rotation	**Observations**	
	PS (d.nm)	**% EE**
500	353.5 ± 5.55	50.02 ± 2.19
1000	214.3 ± 6.31	58.48 ± 1.86
1500	248.3 ± 5.87	44.53 ± 3.15
2000	365.6 ± 6.99	42.64 ± 1.97
Selection of stirring time		
Stirring time	**Observations**	
	PS (d.nm)	**% EE**
0.5	298.3 ± 4.63	42.17 ± 1.63
1.0	261.7 ± 5.15	52.04 ± 1.47
2.0	220.8 ± 4.12	57.41 ± 1.39
3.0	252.7 ± 5.58	52.22 ± 2.53

(n=3, ± S.D.)

8.12.4. Screening and optimization of formulation parameters for PECN preparation:

The results of screening and optimization of formulation parameters such as chitosan concentration, chitosan:chondroitin sulfate ratio and pH of chitosan solution are shown in table- 8.6.

Table- 8.6. Effect of formulation parameters on preparation of RSNa loaded PECN

Chitosan concentration (mg/mL)		
Chitosan concentration (mg/mL)	**Observations**	
	PS (d.nm)	**% EE**
1	174.3 ± 3.48	47.19 ± 2.41
2	199.8 ± 4.12	59.80 ± 2.96
3	230.8 ± 6.12	54.86 ± 1.36
4	305.3 ± 5.59	46.84 ± 0.58
6	396.5 ± 6.34	26.73 ± 3.33
Chitosan:chondroitin sulfate ratio		
Chitosan:chondroitin sulfate ratio	**Observations**	
	PS (d.nm)	**% EE**
0.5:1	152.3 ± 3.44	60.15 ± 1.74
1:1	163.8 ± 3.86	63.98 ± 0.98
1.5:1	192.8 ± 3.47	61.45 ± 1.22
2:1	248.5 ± 5.14	56.40 ± 1.54
3:1	350.1 ± 4.36	45.20 ± 2.01
4:1	362.4 ± 6.66	44.99 ± 2.24
5:1	522.8 ± 8.12	48.26 ± 2.63
6:1	721.8 ± 12.05	45.85 ± 2.15
pH of chitosan solution		
pH of chitosan solution	**Observations**	
	PS (d.nm)	**% EE**
3	232.2 ± 4.18	57.10 ± 1.42
4	198.8 ± 4.12	59.58 ± 1.69
5	273.3 ± 2.94	43.54 ± 1.22
6	353.7 ± 4.65	38.04 ± 2.48
7	314.3 ± 5.81	38.48 ± 1.35

(n=3, ± S.D.)

a. Screening of chitosan concentration:

The chitosan concentration showed a significant effect on particle size as well as EE. The results showed that the particle size increased as the concentration of chitosan increased. The effect of chitosan concentration on EE showed that an increase in concentration of chitosan increased EE up to a certain level and then decreased it with an increase in concentration. It happened due to the larger particle size owing to the relatively loose network within nanoparticles because higher concentration leads to more repulsion among chitosan molecules and leaching of drug from PECN resulting in decrease in drug entrapment [2, 8]. Hence, a concentration range of 1 to 3 mg/mL of chitosan was selected for further optimization.

b. Screening of chitosan:chondroitin sulfate (CS:CHON) ratio:

The CS:CHON ratio is a critical formulation parameter in the preparation of drug-loaded PECN, which showed significant effects on PS and EE. As the CS:CHON ratio decreased, particle size decreased and EE increased. This observation might be attributable to more NH_3^+ groups being neutralized by the CHON negative charge, and eventually decreasing the particle size and forming tightly aggregated nanoparticles, which prevent the leakage of drug from nanoparticles and result in an increase in entrapment efficiency [6]. Hence, 1:1 to 3:1 CS:CHON ratio was selected for further optimization.

c. pH of chitosan solution:

The pH of the chitosan solution showed a significant effect on PS and EE. As pH of chitosan solution increased from 3 to 4, it resulted in decreased PS and increased EE. The explanation behind that, at lower pH, the amino group of CS becomes more protonated, inducing chain repulsion and CHON chain expansion, leading to formation of larger particles. The effect of pH showed that an increase in pH from the 4 to 7, resulted in increased particle size and decreased EE due to the chitosan molecules becoming rarely protonated at higher pH values, which can lead to increased repulsion between the chains due to lower electrostatic interactions, resulting in a more porous structure and a lower entrapment efficiency due to leaching of drug [30, 31]. There was no remarkable change observed in PS or EE at pH 6 or 7. Hence, the 4 to 6 range of pH was selected for further optimization.

Using a design of experiment technique, the high-risk parameters were optimised while keeping other process and formulation variables constant.

8.13. Experimental design and analysis of results:

The RSNa loaded PEC nanoparticles were prepared and optimized by BBD. The design matrix of 16 experimental runs with their responses are shown in table- 8.7. The quadratic model was found to be best fit for all responses and the predicted and observed values were found to be very close to each other. The polynomial equations were generated which explained the individual main effects and interaction effects of independent factors on each dependent variables by Design-Expert V.13.0 version software (Stat-Ease, Inc., USA). All the batches were prepared in triplicate and evaluated for particle size and entrapment efficiency.

Table– 8.7. Experimental runs of RSNa loaded PECN by BBD

Run	Factor 1	Factor 2	Factor 3	Response 1	Response 2
	A: Chitosan Concentration mg/ml	B: CS:CHON Ratio	C: pH	Particle Size (d.nm)	EE (%)
R1	1	2:1	4	243.3 ± 5.87	31.92 ± 2.29
R2	2	1:1	4	173.2 ± 3.14	61.46 ± 1.61
R3	2	1:1	6	275.9 ± 5.15	40.72 ± 1.24
R4	2	2:1	5	257.4 ± 6.78	51.62 ± 1.10
R5	3	2:1	6	385.2 ± 5.33	31.57 ± 2.74
R6	1	3:1	5	293.2 ± 4.51	33.61 ± 1.69
R7	2	3:1	6	300.9 ± 4.44	41.42 ± 1.47
R8	1	1:1	5	242.4 ± 5.96	41.07 ± 1.44
R9	2	2:1	5	261.3 ± 6.18	51.27 ± 2.58
R10	2	2:1	5	265.5 ± 6.16	54.08 ± 2.04
R11	3	2:1	4	273.8 ± 5.11	43.86 ± 2.39
R12	2	3:1	4	254.9 ± 4.13	35.63 ± 1.56
R13	3	3:1	5	400.6 ± 4.36	38.31 ± 1.02
R14	3	1:1	5	325.8 ± 4.58	47.75 ± 0.89
R15	1	2:1	6	280.2 ± 5.15	24.19 ± 1.32
R16	2	2:1	5	244.5 ± 4.26	49.16 ± 1.20

(n=3, ± S.D.)

The effect of independent variables on responses are discussed below:

8.13.1. Effects of independent variables on particle size:

The values of particle size varied from 173.2 to 400.6 d.nm throughout all 16 runs due to variation in independent factor combinations. From the statistical analysis, we can observe that R^2 value for actual Vs predicted values for particle size was 0.8402 which is good correlation.

ANOVA results of model:

A summary of the ANOVA results of different models for particle size is shown in the table- 8.8, which depicts the model p-value with adjusted and predicted R^2 values.

Table- 8.8. Summary of ANOVA results of different model for particle size

Source	Sequential p-value	Lack of Fit p-value	Adjusted R^2	Predicted R^2	
Linear	0.0025	0.0168	0.6038	0.3790	
2FI	0.6430	0.0125	0.5573	-0.1804	
Quadratic	**0.0004**	**0.3321**	**0.9630**	**0.8402**	**Suggested**
Cubic	0.3321		0.9729		**Aliased**

Based on the results obtained from the experiments and criteria of lowest p-value ($p<0.05$), quadratic model was suggested to be best fitted to the observed responses. The significant and insignificant terms are classified based on p value, which means those models with p-values less than 0.05 are significant, while others are insignificant [32].

The ANOVA results of quadratic model for particle size is shown in table- 8.9. The **Model F-value** of 44.34 implies the model is significant. There is only a 0.01% chance that an F-value this large could occur due to noise. The **P-values** less than 0.0500 indicate model terms are significant. In this case A, B, C, AC, BC, A^2 are significant model terms. The **F-value** for **lack of fit** was found to be 1.73, which implies that the lack of fit was not significant relative to the pure error. There is a 33.21% chance that a Lack of Fit F-value this large could occur due to noise. Non-significant lack of fit was good for the model to fit.

Table- 8.9. ANOVA results of quadratic model for particle size

Source	Sum of Squares	df	Mean Square	F-value	p-value	
Model	44829.04	9	4981.00	44.34	< 0.0001	Significant
A-Chitosan Concentration	13308.96	1	13308.96	118.48	< 0.0001	
B-CS:CHON Ratio	6745.41	1	6745.41	60.05	0.0002	
C-pH	11026.12	1	11026.12	98.16	< 0.0001	
AB	144.00	1	144.00	1.28	0.3007	
AC	1387.56	1	1387.56	12.35	0.0126	
BC	803.72	1	803.72	7.16	0.0368	
A^2	10552.43	1	10552.43	93.94	< 0.0001	
B^2	193.91	1	193.91	1.73	0.2369	
C^2	666.93	1	666.93	5.94	0.0507	
Residual	673.96	6	112.33			
Lack of Fit	426.93	3	142.31	1.73	0.3321	Not significant
Pure Error	247.03	3	82.34			
Cor Total	45503.00	15				

Table- 8.10. Summary of ANOVA results for particle size

Parameters	Results	Parameters	Results
Std. Dev.	10.60	**R^2**	0.9852
Mean	279.88	**Adjusted R^2**	0.9630
C.V. %	3.79	**Predicted R^2**	0.8402
		Adeq Precision	26.4089

The **Predicted R^2** of 0.8402 is quite close to the **Adjusted R^2** of 0.9630, with a difference of less than 0.2 (shown in table 8.10). The signal-to-noise ratio was determined using the Adeq Precision. A ratio of 26.409 (higher than 4 is preferable) indicated a signal of adequate quality. As a result, this model will be utilized to explore the design space.

Model diagnostic plots:

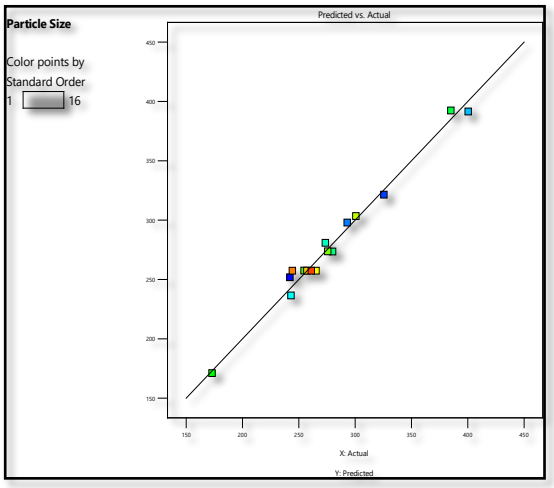

a. Predicted Vs actual

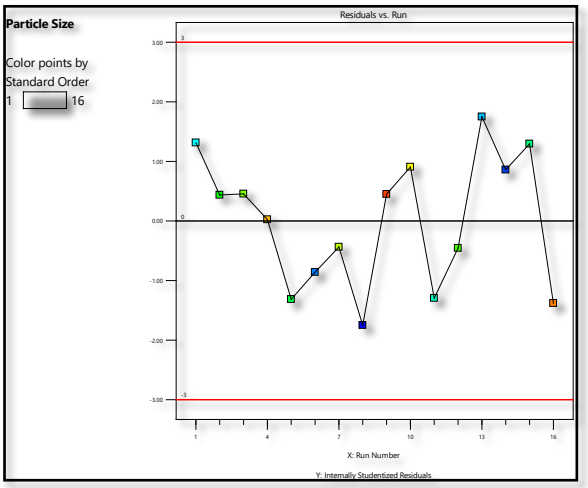

b. Residual vs run

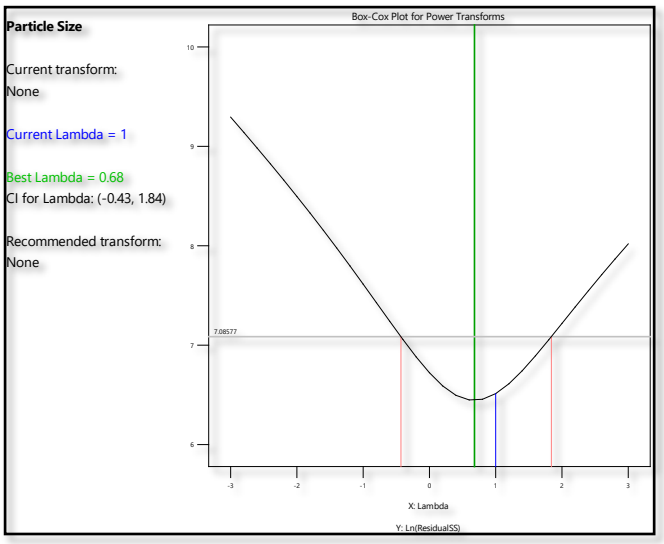

c. Box-Cox plot for power transforms

Figure– 8.2. Model diagnostic plots for particle size

a. Predicted Vs actual plot
b. Residual vs run plot
c. Box-Cox plot for power transforms

Various diagnostic plots for evaluation of model are shown in figure- 8.2. The predicted vs. actual plot (a) follows a 45° straight line, indicating a close relation between actual and predicted values. The residual versus run plot (b) in the present investigation showed a random distribution of residuals, indicating the lack of any lurking variable. The Box-Cox plot for power transformation (c) showed the current λ value of 1, which

lies nearer to the best λ values (0.68) indicating that there was no requirement for any power transformation.

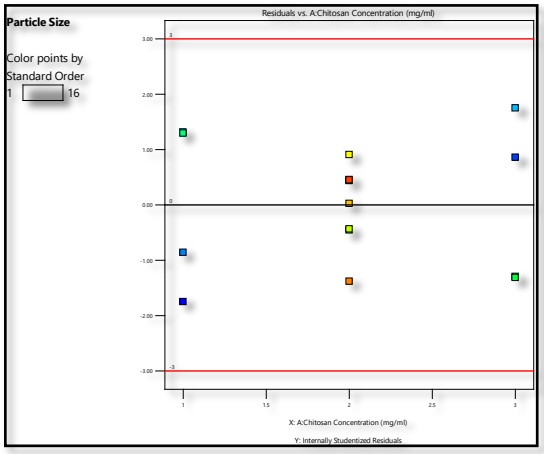

a. Residual Vs Chitosan concentration

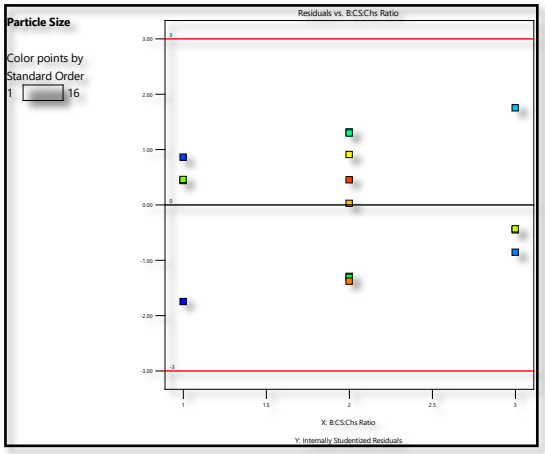

b. Residual Vs CS:CHON ratio

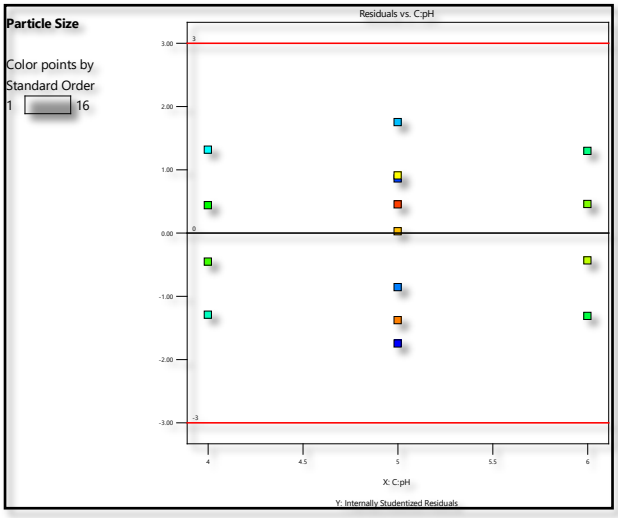

c. Residual Vs pH of chitosan solution

Figure- 8.3. Residual Vs factor plots

a. Residual Vs Chitosan concentration
b. Residual Vs CS:CHON ratio
c. Residual Vs pH of chitosan solution

The plots for residual vs each factor, are shown in the figure- 8.3. The figure showed random scattered throughout the increasing level of factors, demonstrating that the model is effective in accounting for the variation in different levels of each variable.

Model plots: Response surface plot (3D plot):

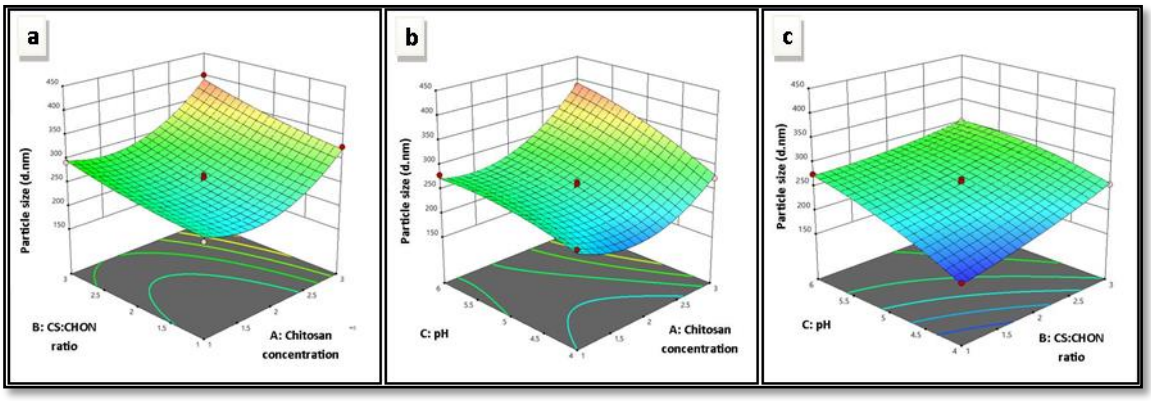

Figure- 8.4. 3D surface plot for particle size.

a. Chitosan concentration and CH:CHON ratio
b. Chitosan concentration and pH of chitosan solution
c. CH:CHON ratio and pH of chitosan solution

The 3D surface plot (Figure- 8.4a) and positive magnitude of factor A (equation-8.5) revealed that as the concentration of chitosan increased, the particle size also increased due to the increase in density of protonated amino groups, and at higher chitosan concentration, hydrogen bonding overcomes the electrostatic attraction, causes greater repulsion among them, and leads to an increase in particle size. At low concentration of chitosan, electrostatic forces between sulfate, and carboxylate anions and protonated amine groups of chitosan predominated over the attractive forces created by the intermolecular hydrogen bonding between chitosan group resulted in decreased in particle size [6].

The 3D surface plot (figure- 8.4b) and positive magnitude of factor B (equation-8.5) revealed that the particle size increased with increasing CS:CHON ratio. This could be due to more NH_3^+ groups being neutralised by the CHON negative charge and the repulsion of the chitosan molecules being overcome, resulting in particle size reduction [6, 8]. At higher ratio, the excess chitosan molecules increased the intermolecular attraction forces between chitosan molecule and resisted the electrostatic attraction force between CHON anions and NH_3^+ cations, resulted in the increasing particle size diameter [6].

The 3D surface plot (figure- 8.4c) and positive magnitude of factor C (equation-8.5) revealed that an increase in pH of chitosan solution results in an increase in particle size, showing a positive correlation with pH of chitosan solution. At pH 4.0 to 5.0 in the chitosan

solution, predominant ions of chitosan existed in the solution, which formed complex with oppositely charged CHON ions effectively and allow the production of nanoparticles with good crosslinking and small particle size [4, 6].

Polynomial equation for Particle size:

The polynomial equations were obtained from design for particle size as follows:

Final equation in terms of coded factors:

$$\text{Particle Size (d.nm)} = +257.18 + 40.79 * A + 29.04 * B + 37.13 * C + 6.00 * AB + 18.62 * AC - 14.18 * BC + 51.36 * A^2 + 6.96 * B^2 - 12.91 * C^2$$

……..equation- 8.5

Reduced equation in terms of coded factors:

$$\text{Particle Size (d.nm)} = +257.18 + 40.79 * A + 29.04 * B + 37.13 * C + 18.62 * AC - 14.18 * BC + 51.36 * A^2$$

……..equation- 8.6

8.13.2. Effects of variables on % EE:

The values of entrapment efficiency varied from 24.19 to 61.46 % throughout all 16 runs due to variation in independent factor combination. From the statistical analysis, we can observe that R^2 value for actual Vs predicted values for % EE was 0.7456 which is good correlation.

Table- 8.11. Summary of ANOVA results of different models for % EE

Source	Sequential p-value	Lack of Fit p-value	Adjusted R^2	Predicted R^2	
Linear	0.1586	0.0109	0.1755	-0.1590	
2FI	0.5704	0.0086	0.1109	-0.7985	
Quadratic	**0.0002**	**0.3537**	**0.9450**	**0.7682**	**Suggested**
Cubic	0.3537		0.9578		**Aliased**

Summary of ANOVA results of different models for % EE is shown in table- 8.11. The polynomial with lowest p values (<0.05) was considered for model selection. On the basis of criteria, the quadratic model was found to be best fitted to the observed responses and chosen for further evaluation.

Table- 8.12. ANOVA results of design model for % EE

Source	Sum of Squares	df	Mean Square	*F-value*	p-value	
Model	1412.15	9	156.91	29.65	0.0003	**Significant**
A-Chitosan Concentration	117.81	1	117.81	22.26	0.0033	
B-CS:CHON Ratio	220.82	1	220.82	41.72	0.0007	
C-pH	152.86	1	152.86	28.88	0.0017	
AB	0.9801	1	0.9801	0.1852	0.6820	
AC	5.20	1	5.20	0.9822	0.3599	
BC	175.96	1	175.96	33.25	0.0012	
A^2	541.49	1	541.49	102.31	< 0.0001	
B^2	0.3306	1	0.3306	0.0625	0.8110	
C^2	196.70	1	196.70	37.17	0.0009	
Residual	31.76	6	5.29			
Lack of Fit	19.56	3	6.52	1.60	0.3537	Not significant
Pure Error	12.20	3	4.07			
Cor Total	1443.91	15				

The ANOVA results of design model for % EE is shown in table- 8.12. The **Model F-value** of 29.65 implies the model is significant. There is only a 0.03% chance that an F-value this large could occur due to noise. In this case, A, B, C, BC, A^2, C^2 are significant model terms ($p<0.05$). The **F-value** for **lack of fit** was found to be 1.60, which implies that the lack of fit was not significant ($p>0.05$) relative to the pure error.

There is a 35.37% chance that a Lack of Fit F-value this large could occur due to noise. Non-significant lack of fit is good for model to fit.

Table- 8.13. Summary of ANOVA results for % EE

Parameters	Values	Parameters	Values
Std. Dev.	2.30	**R^2**	0.9780
Mean	42.35	**Adjusted R^2**	0.9450
C.V. %	5.43	**Predicted R^2**	0.7682
		Adeq Precision	19.3808

The **Predicted R^2** of 0.7682 is in reasonable agreement with the **Adjusted R^2** of 0.9450; i.e. the difference is less than 0.2 (shown in table- 8.13). **The Adeq Precision** measures the signal to noise ratio. The ratio of 19.3808 (greater than 4 is desirable) indicates an adequate signal. This model can be used to navigate the design space.

Model diagnostic plots:

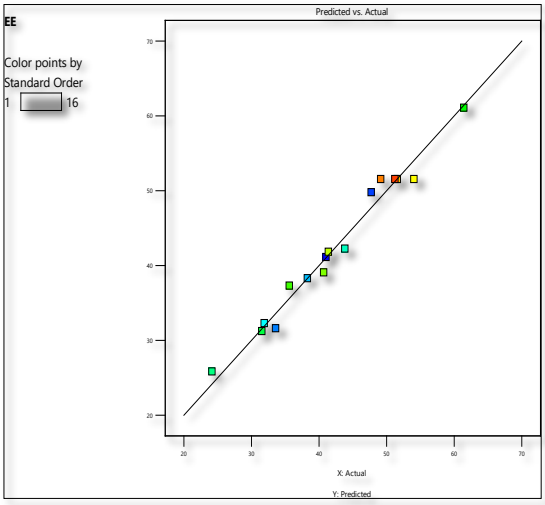

a. Predicted Vs actual

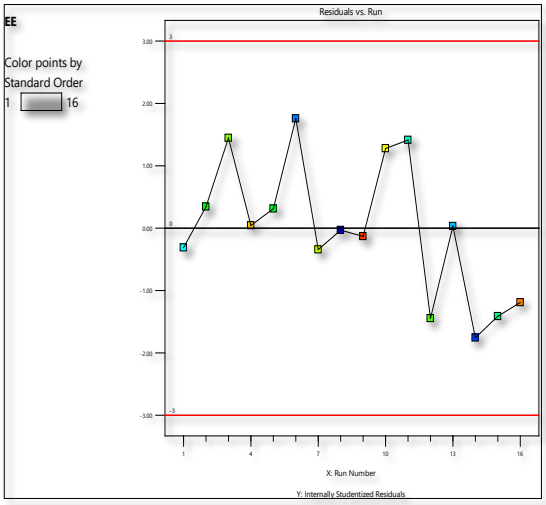

b. Residual vs run

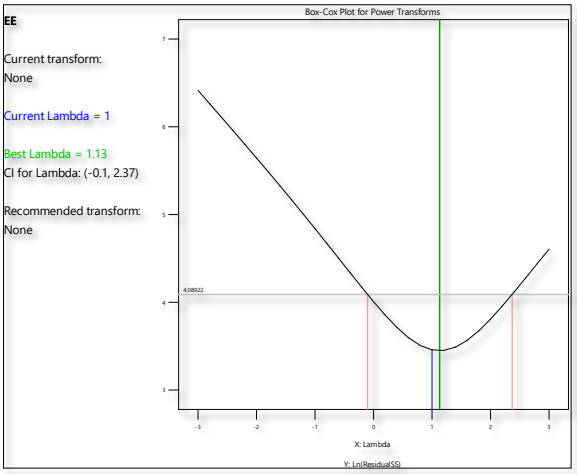

c. Box-Cox plot for power transforms

Figure- 8.5. Model diagnostic plots for % EE

a. Predicted Vs actual plot
b. Residual vs run plot
c. Box-Cox plot for power transforms

Various diagnostic plots for evaluation of model are shown in figure- 8.5. The **predicted vs actual plot (a)** follows a 45° straight line which indicates a close estimation of actual values with predicted values. The **residual vs. run plot (b)** shows a random distribution of residuals in the current analysis, indicating the absence of any lurking variables. The **Box-Cox plot** (c) showed the current λ value of 1, which lies nearer to the best λ values (1.13) indicating that there was no requirement for any power transformation.

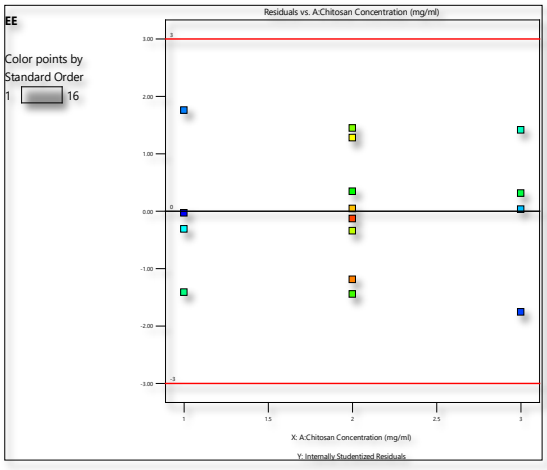

a. Residuals Vs Chitosan concentration

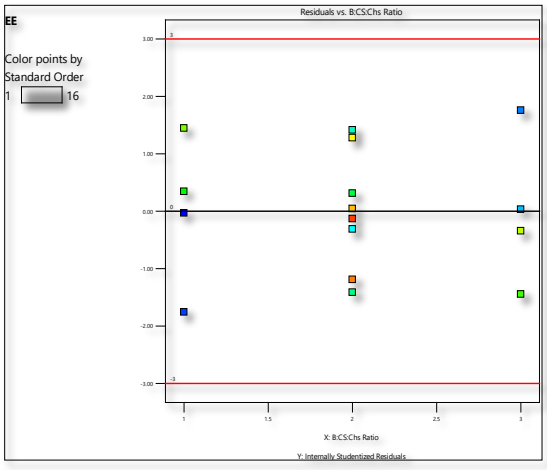

b. Residuals Vs CS:CHON ratio

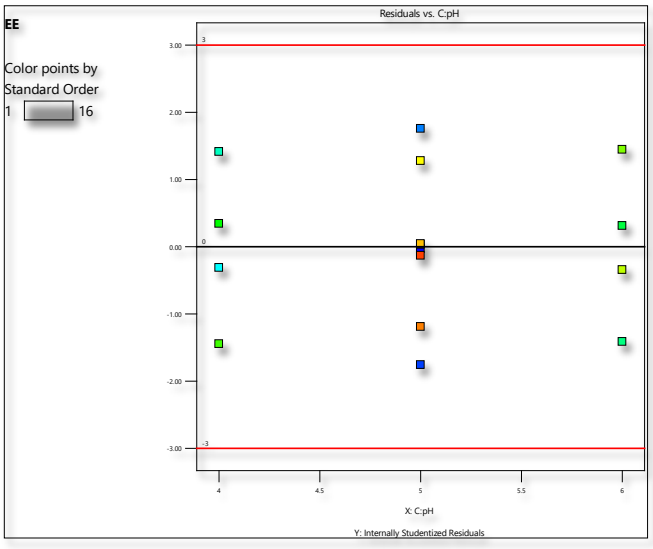

c. Residuals Vs pH of chitosan solution

Figure- 8.6. Residual Vs factor plots

a. Residuals Vs Chitosan concentration
b. Residuals Vs CS:CHON ratio
c. Residuals Vs pH of chitosan solution

The plots for residuals with each factor (shown in figure- 8.6) represents random scattered throughout the increasing level of factors, demonstrating that the model is effective in accounting for the variation in different levels of each variable.

Model Plots: Response surface plot (3D)

The ANOVA data indicate which variables have a significant influence on entrapment efficiency, as seen in the response surface 3D plot (shown in figure- 8.7).

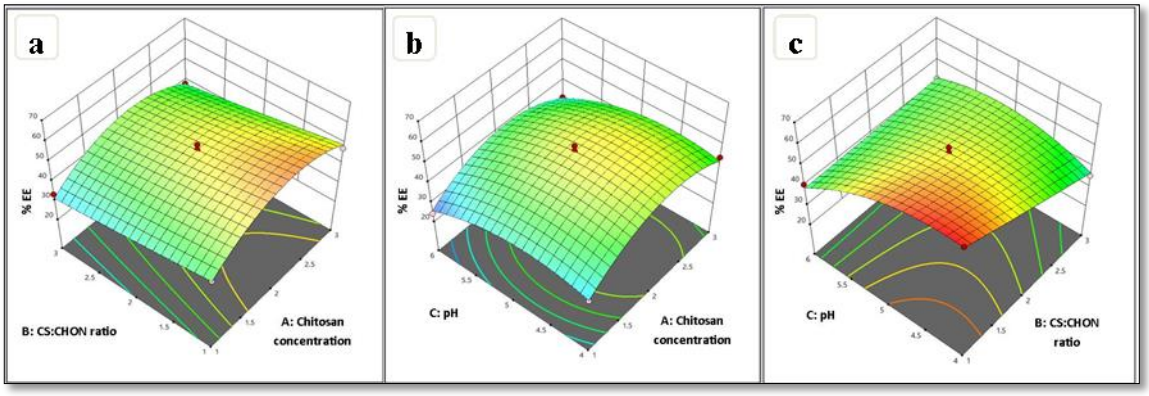

Figure- 8.7. 3D surface plot for showing effects of independent factors on % EE.

a. Chitosan concentration and CS:CHON ratio
b. Chitosan concentration and pH of chitosan solution
c. CS:CHON ratio and pH of chitosan solution

The 3D surface plot and positive magnitude of factor A (equation-8.7a) showed positive correlation of chitosan concentration with % EE. The results showed that an increase in the concentration of chitosan increases the % EE, which may be attributed to the relative increase in the amount of polymer, leading to more polymeric network spaces for drug entrapment [33, 34].

The 3D surface plot and negative magnitude of factor B (equation-8.7b) revealed that the increase in CS:CHON ratio results in decrease in % EE attributed to inadequate interaction of chitosan and chondroitin sulfate allow the drug leach out from the loosely aggregated polyelectrolyte nanoparticles resulted in lowering EE [35]. This lowered EE with increase in CS:CHON ratio may be caused by the fact that when chitosan concentration increased with respect to CHON resulted in particle aggregation due to lack of availability of an opposing charge react with CHON which form porous structured PECN leads to leaching of drug [1, 33].

The entrapment efficiency decreased as the pH of the chitosan solution increased (figure-8.7c). When the pH increased to 6.0, most of the amine groups in CS were rarely protonated at all, resulting in lower electrostatic interactions and loose tangling, and therefore the leaching of the drug from nanoparticles was increased resulting in lower EE [36]. In contrast, at higher pH, increase in particle size observed leads to reduction in the surface area of nanoparticles, which decreases drug entrapment efficiency [2, 30]. At pH 4, the chitosan easily crosslinked with the CHON, due to

more charge NH3+ group of CS efficiently interacted with -OSO3- group of CHON (≈ 70% ionized at pKa of 2.6) resulted in the higher production of PECN allowing more drug to be entrapped inside nanoparticles [37].

The polynomial equations obtained from design for entrapment efficiency are as follows:

$$\text{Entrapment Efficiency (\%)} = +51.53 + 3.84 * A - 5.25 * B - 7.15 * C + 0.4950 * AB - 1.14 * AC + 6.63 * BC - 11.64 * A^2 + 0.2875 * B^2 - 7.01 * C^2$$

……equation- 8.7

Reduced equation in terms of coded factors:

$$\text{Entrapment Efficiency (\%)} = +51.53 + 3.84 * A - 5.25 * B - 7.15 * C + 6.63 * BC - 11.64 * A^2 - 7.01 * C^2$$

……equation- 8.8

8.14. Desirability plot and overlay plot for optimization:

Table- 8.14 shows the desirable batch parameters.

Table- 8.14. Variables for desirability plot and goals for response

Name	Goal	Lower Limit	Upper Limit
A: Chitosan Concentration (mg/mL)	Is in range	1	3
B: CS:CHON Ratio	Is in range	1:1	3:1
C: pH of chitosan solution	Is in range	4	6
Particle Size (d.nm)	Minimize	173.2	400.6
EE (%)	Maximize	24.19	61.46

The ramp graph (figure-8.8 c) shows the projected values of both responses for the optimal concentration of independent variables, while the bar graph (figure-8.8b) shows

individual desired value for particle size (0.980) and % EE (1.00). The projected answer has a composite desirability of 0.990 (shown in figure- 8.8c).

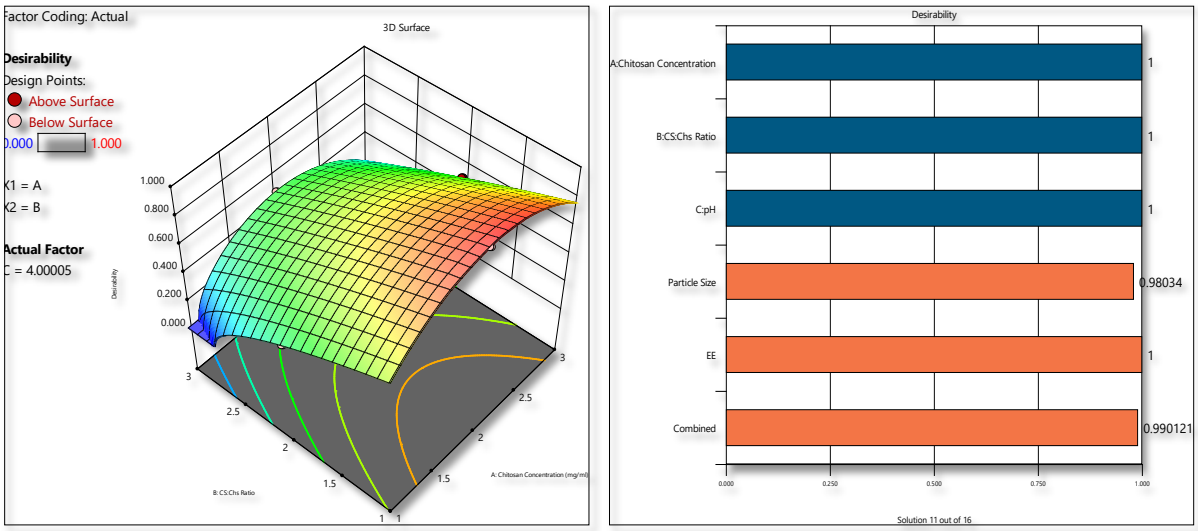

a. 3D Desirability plot

b. Bar graph of desirability

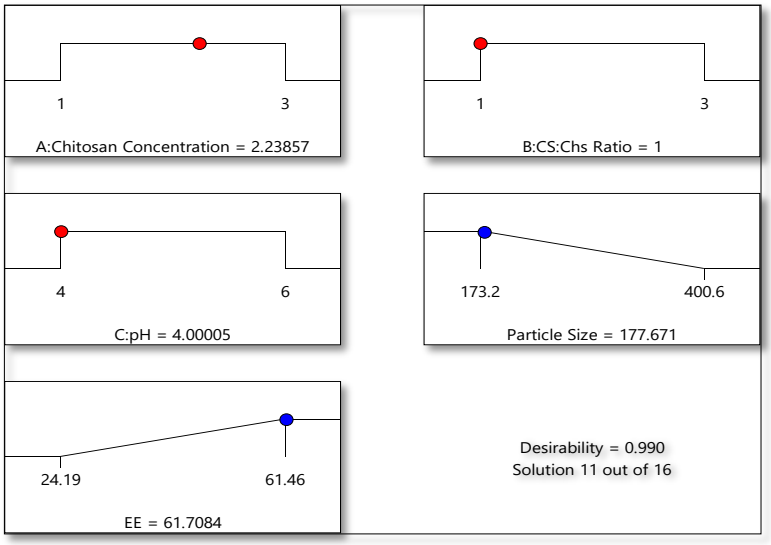

c. Ramp graph of desirability

Figure- 8.8. Desirability plot for RSNa loaded PECN

a. 3D desirability plot

b. Bar graph of desirability

c. Ramp graph of desirability

To evaluate the desirability, RSNa loaded PECN formulation was prepared according to the suggested batch, and the obtained response values were determined to be similar with the predicted responses. Furthermore, the design's error was determined to be less than

5%, indicating its eligibility for prediction. This demonstrates that the software-predicted optimum formulation is reliable for practical purposes.

8.15. Assessment of the optimized RSNa loaded PECN:

Based on the criteria of maximum entrapment efficiency and minimum particle size, the optimized batch of RSNa loaded PECN obtained from the design space plot was prepared to confirm the reliability of optimization design. The suggested optimized nanoparticles composition and their responses are shown in table- 8.15. The observed data was found to be aligned with the predicted values. The minimum % error was found between observed values and predicted values with no significant difference ($p<0.05$) showing the Box-Behnken design's reliability and efficiency.

Table-8.15. Predicted and observed responses of optimized RSNa loaded PECN

Variables	Values	Responses	Predicted values	Observed values	% Error
Chitosan concentration (mg/mL)	2.24	**PS (d.nm)**	177.66	171.6 ± 4.68	3.44
CS:CHON Ratio	1:1	**EE (%)**	61.70	61.13 ± 2.19	0.92
pH of Chitosan solution	4.0				

(n=3, ± S.D.)

8.16. Graphical optimization to generate control space:

Figure- 8.9 shows the design overlay plot. This overlay plot was obtained by superimposing counter plots of both responses in the factor space, which displaces the region of feasible response values. The upper and lower ranges of the desired responses were selected for the generation of the overlay plot. The yellow area inside each plot shows the range of independent variables where the criteria for both response variables are satisfied.

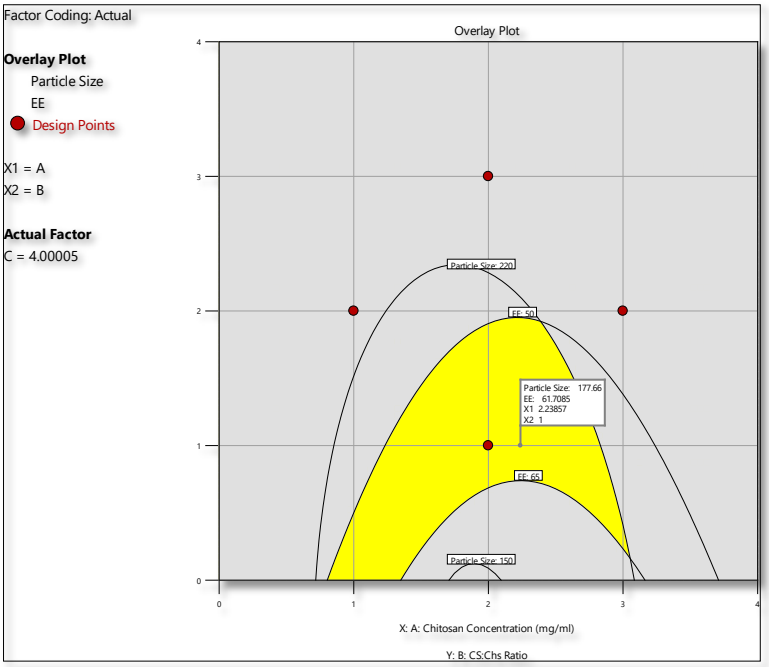

Figure- 8.9. Overlay plot for design space

8.17. Analysis of design space:

To assess the robustness of the design space, three formulations were selected at random from the plotted design space (shown in figure- 8.10). The formulation was prepared using the provided factor values, and the predicted and actual response values were compared.

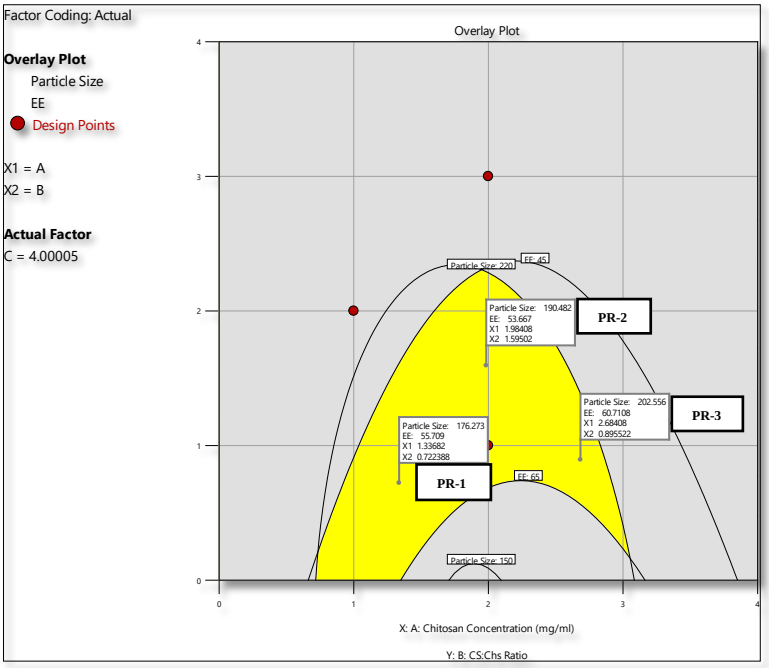

Figure- 8.10. Analysis of design space

Table- 8.16. Check point batch analysis

Formulation	Parameters	Predicted	Observed	Std. Error
PR-1	**PS (d.nm)**	176.27	178.4 ± 7.15	1.20
	% EE	55.70	57.30 ± 1.99	2.87
PR-2	**PS (d.nm)**	190.48	184.4 ± 5.84	3.19
	% EE	53.66	51.86 ± 2.68	3.35
PR-3	**PS (d.nm)**	202.56	195.5 ± 4.19	3.44
	% EE	60.71	58.14 ± 1.15	4.23

(n=3, ± S.D.)

According to the robustness analysis (shown in table- 8.16), the observed responses remained within the boundary, and the variation between predicted and observed values was not significant.

8.18. Point prediction and confirmation:

The optimised response values were validated by doing the experiment in triplicate with the selected factor values. On the basis of the results, it was found that the observed and predicted values were in good agreement, indicating the suitability of the proposed model for optimization (shown in table- 8.17).

Table- 8.17. Predicted responses for selected solution along with standard deviation

Analysis	Predicted Mean	Observed	Std Dev	n	95% PI low	95% PI high
PS (d.nm)	177.66	171.6 ± 4.68	10.59	3	154.88	200.45
% EE	61.70	61.13 ± 2.19	2.30	3	56.76	66.65

(n=3, ± S.D.)

8.19. Physicochemical characteristics of RSNa loaded PECN:

8.19.1. Particle size, % EE, % drug loading capacity and surface charge analysis:

The average particle size of optimized RSNa loaded PECN was found to be 171.6 ± 4.68 d.nm with 0.280 ± 0.127 PDI (shown in figure- 8.11). The % EE was found to be

61.13 ± 2.19 % with % loading capacity of 13.23 ± 0.39 %. The surface charge of RSNa loaded PECN was found to be 21.25 ± 2.18 mV (shown in figure- 8.12). Nanoparticles with a high positive zeta potential offer good physical stability due to electrostatic repulsion of individual particles [7, 38].

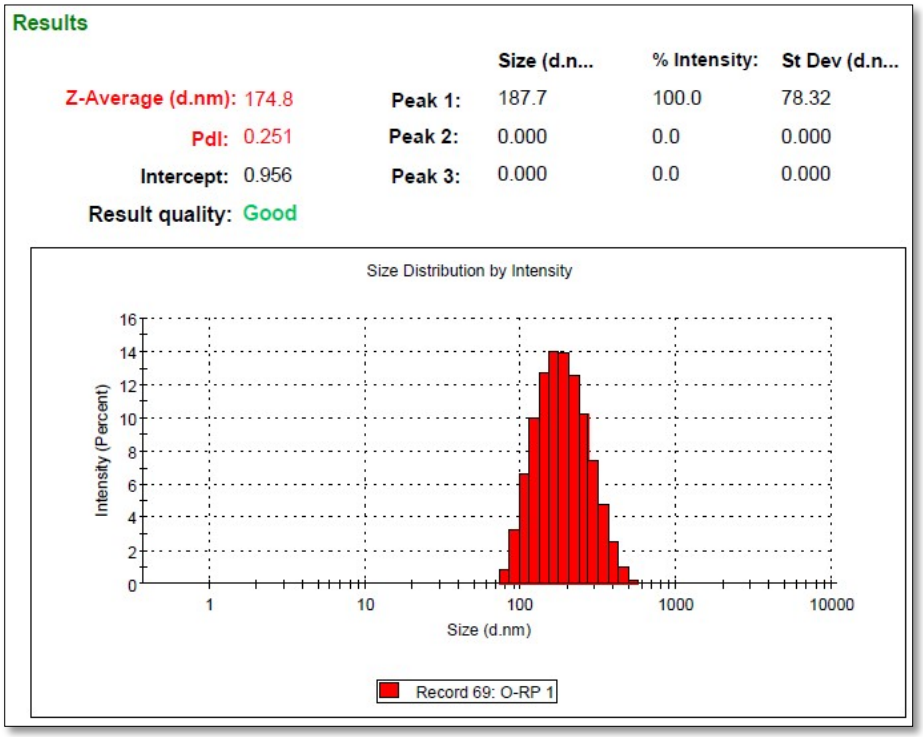

Figure- 8.11. Particle size analysis by zetasizer

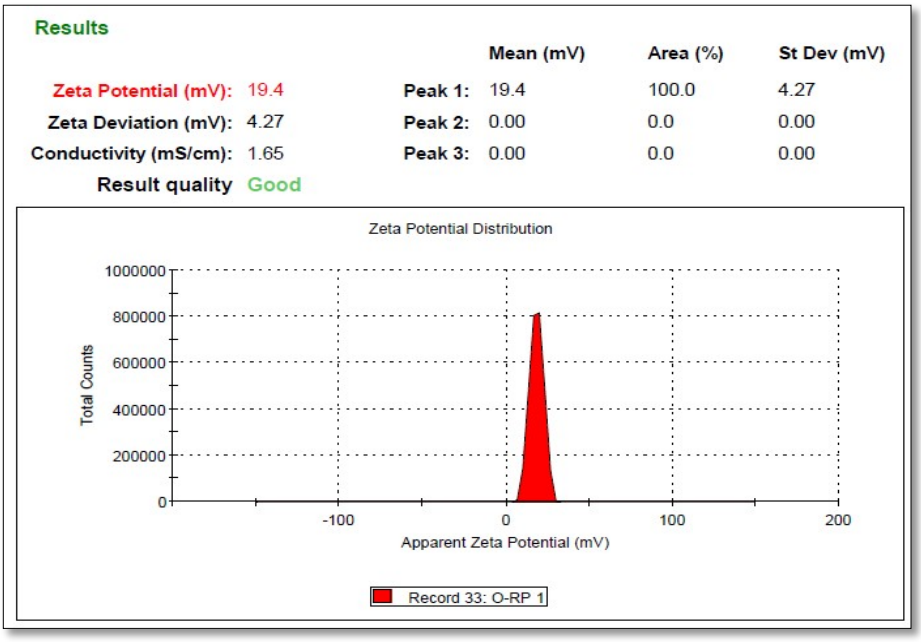

Figure- 8.12. Zeta potential analysis by zetasizer

8.19.2. Surface morphological analysis:

The surface morphological analysis of optimized RSNa loaded PECN is shown in figure- 8.13. Figure- 8.13 depicts well defined spherical shape with homogenously dispersed particle with size less than 200 nm. The TEM image showed good particle integrity indicating strong interactions between chitosan and chondroitin sulfate.

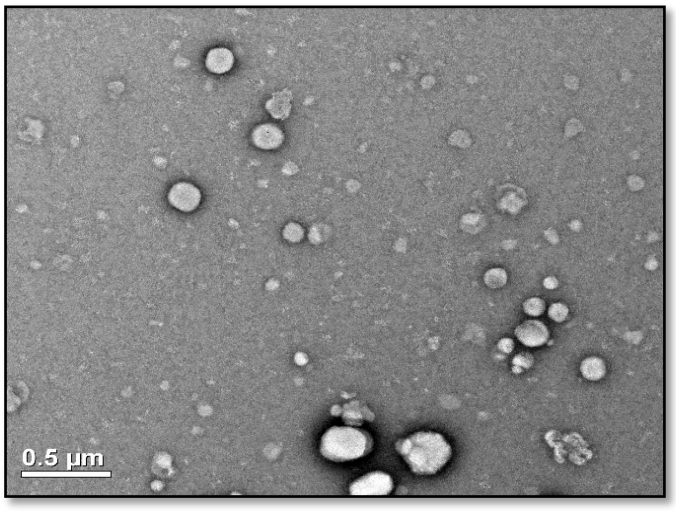

Figure- 8.13. TEM analysis of RSNa PECN

8.19.3. FTIR analysis:

The compatibility of RSNa with excipients in the PEC nanoparticles was confirmed through their spectral analysis. The FTIR spectra of RSNa and RSNa loaded PECN are shown in figure-8.14. The RSNa spectrum showed distinct peak in region of hydroxyl group which is associated with the O=P-OH in the spectral region of 1585-1740 cm^{-1} and found at 1652.5 cm^{-1}. The characteristic peaks of phosphate group (P=O stretching) were observed within range of 910-1040 cm^{-1} and found at 931.62 cm^{-1}. The CO-H vibration corresponding to -OH groups was observed at 3363.56 cm^{-1}. There was negligible change observed in the frequencies and intensity of characteristics peak in RSNa loaded PECN. Hence, it was concluded that the RSNa is maintaining its structural integrity and compatibility with excipients confirmed.

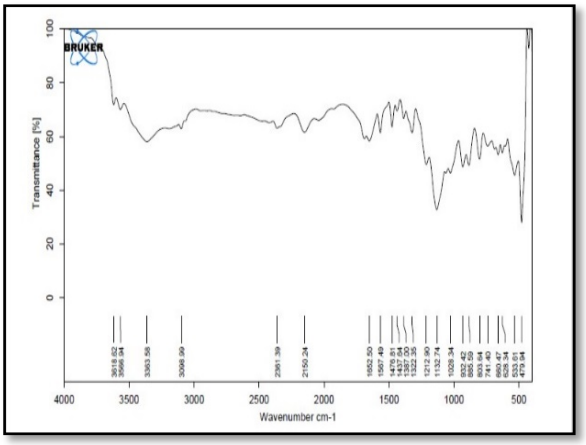

Figure- 8.14A. FTIR spectra of RSNa

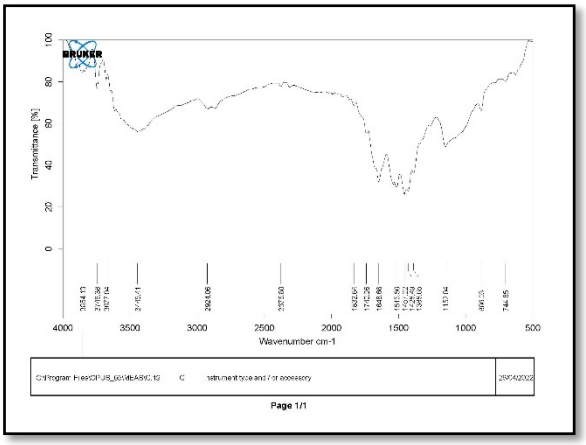

Figure- 8.14B. FTIR spectra of RSNa loaded PECN

8.19.4. DSC analysis:

Thermograms of pure drug (RSNa) and RSNa loaded PECN are shown in figure- 8.15. The thermogram of pure drug showed an intensive endothermic peak at 253.2 °C, which indicated the crystalline nature of the drug. The peak of RSNa disappeared in thermogram of RSNa loaded PECN confirming that the drug was completely encapsulated in polymer matrix [6].

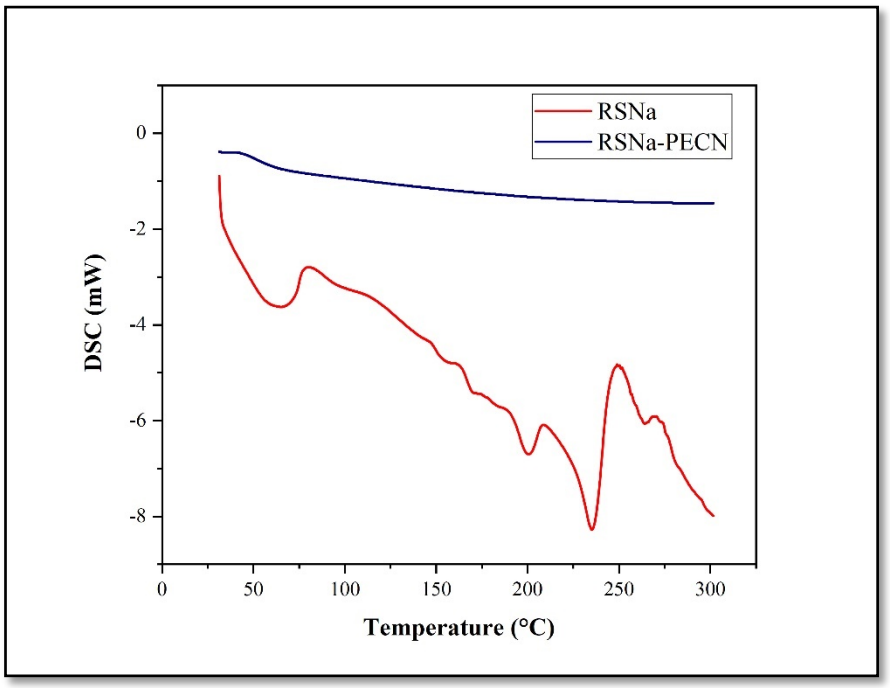

Figure- 8.15. DSC thermogram of RSNa and RSNa-PECN

8.19.5. X-ray diffraction study:

The XRD analysis of RSNa and RSNa loaded PECN is shown in figure- 8.16. The XR diffractogram of RSNa showed the presence of many sharp peaks, indicating its crystalline nature. The XRD profile of RSNa-loaded PECN revealed the disappearance of intense RSNa characteristic peaks, confirming drug encapsulation within polymeric matrix and indicating its amorphous state in the formulation [39].

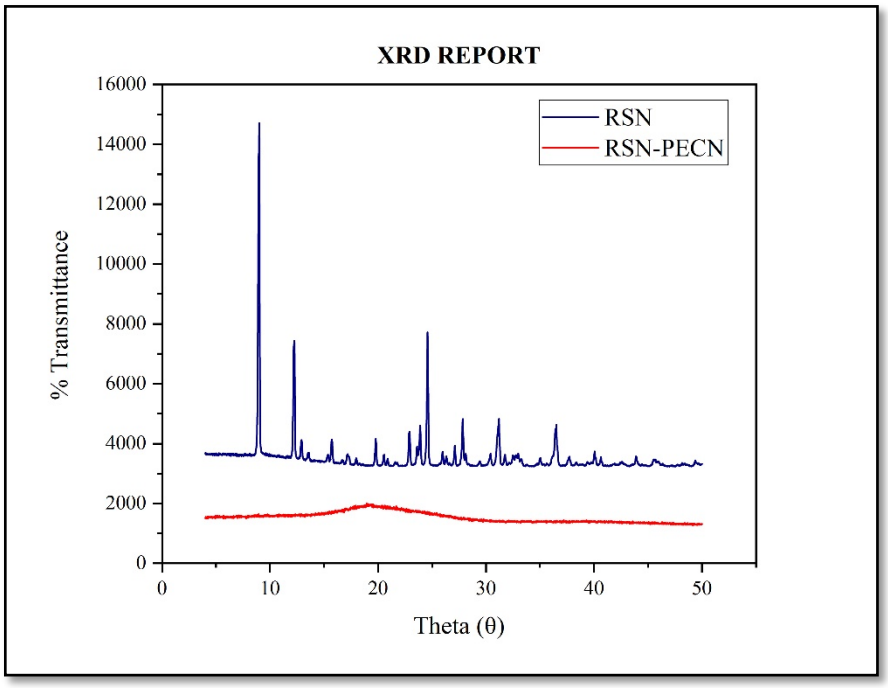

Figure- 8.16. X-ray Diffractogram of RSNa and RSNa-PECN

8.20. In vitro drug release study:

The optimized batch of RSNa loaded PECN and RSNa solution were analyzed for cumulative drug release at physiological blood pH i.e., PBS 7.4 (table- 8.19) and skin pH i.e., PBS 5.5 (table- 8.18) using dialysis bag method (figure- 8.17). The results showed that 99.50% and 98.94% of RSNa were released from RSNa solution in pH 5.5 and pH 7.4 medium, respectively. In case of RSNa loaded PECN, it was found to be 72.79% and 97.41% of RSNa release within 48 hrs in pH 5.5 and pH 7.4 medium, respectively. From the release study, it was observed that RSNa was very slowly released from PECN at pH 5.5 as compared to pH 7.4. The release pattern showed sustained release of RSNa from PECN matrix. The release of RSNa from PECN at pH 5.5 was slower might be due to greater stability of PECN network structure at this pH [6, 34, 40].

The obtained data were fitted in various release model like Zero order, First order, Higuchi and Korsmeyer-Peppas model for both PBS 5.5 (shown in figure- 8.18 and table- 8.20) and PBS 7.4 (shown in figure- 8.19 and table- 8.21). The release from RSNa solution followed zero order kinetic with regression coefficient of 0.9877 and 0.9565 in PBS pH 5.5 and PBS pH 7.4 respectively. The release pattern from RSNa loaded PECN followed Higuchi model with regression coefficient of 0.9846 and 0.9705 in PBS pH 5.5 and PBS pH 7.4 respectively. The release exponent (n) for RSNa solution and RSNa loaded PECN revealed release mechanism of drug from PECN at PBS 5.5 and PBS 7.4 is shown in table- 8.20 and 8.21 respectively. The RSNa loaded PECN followed non-fickian or anomalous mechanism of release in both medium with release exponential value found between 0.45 to 0.85 [41]. Erosion and diffusion were the major mechanism for drug release from nanoparticles. The sustained phase released the drug at a slower rate, which may have been contributed by the diffusion of the entrapped drug inside the polymer's cross-linked matrix [6, 34, 40].

Table- 8.18. In vitro drug release profile for RSNa loaded PECN in PBS pH 5.5

Time (In Hrs)	RSNa solution	RSNa loaded PECN
0	0 ± 0	0 ± 0
0.5	33.57 ± 3.26	0.91 ± 0.38
1	56.50 ± 2.58	2.63 ± 1.24
1.5	81.57 ± 4.96	5.36 ± 1.06
2	96.83 ± 5.53	7.89 ± 1.55
3	99.50 ± 3.32	8.51 ± 1.85
4		13.61 ± 2.55
5		17.21 ± 2.21
6		20.12 ± 1.24
8		28.34 ± 1.96
12		36.07 ± 1.53
24		49.79 ± 2.05
36		57.94 ± 1.59
48		72.79 ± 1.66

(n=3, ±S.D.)

Table- 8.19. In vitro drug release profile of RSNa loaded PECN in PBS pH 7.4

Time (In Hrs)	RSNa solution	RSNa loaded PECN
0	0 ± 0	0 ± 0
0.5	38.99 ± 4.32	6.32 ± 2.54
1	59.51 ± 5.13	11.42 ± 1.11
1.5	75.24 ± 4.52	12.87 ± 1.86
2	84.19 ± 6.43	16.72 ± 2.54
3	98.94 ± 2.02	24.92 ± 2.86
4		32.00 ± 1.23
5		39.72 ± 2.65
6		44.27 ± 2.69
9		53.10 ± 2.12
12		60.68 ± 1.87
24		71.45 ± 3.98
36		89.52 ± 2.56
48		97.41 ± 3.15

(n=3, ±S.D.)

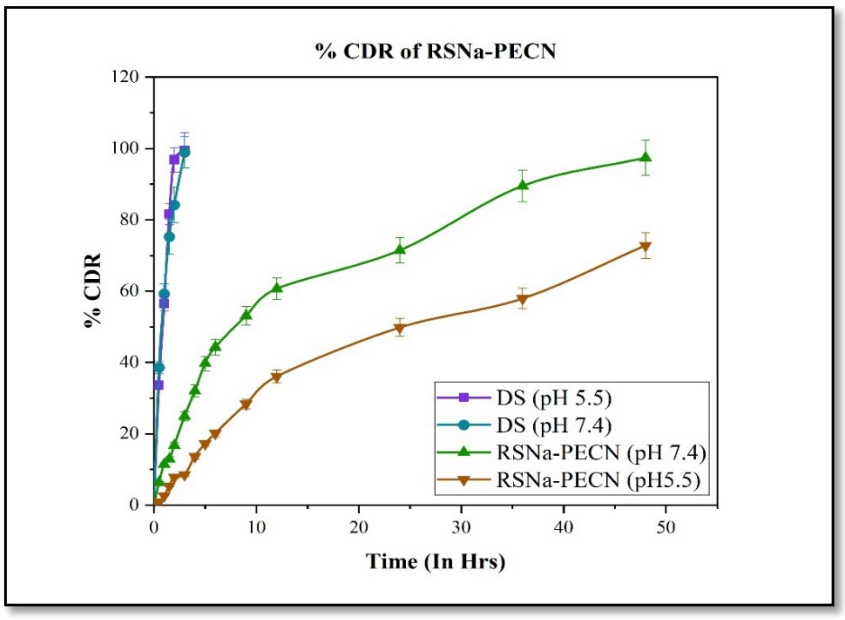

Figure- 8.17. In vitro cumulative drug release profile

Table- 8.20. Drug release kinetic models for RSNa loaded PECN in PBS pH 5.5

Kinetic Models	RSNa solution	RSNa loaded PECN
Zero order	**0.9877**	0.9336
First order	0.8440	0.9829
Higuchi	0.9473	**0.9846**
Korsemeyer-Peppas (n)	0.2372 **(0.543)**	0.7504 **(0.692)**

Table- 8.21. Drug release kinetic models for RSNa loaded PECN in PBS pH 7.4

Kinetic Models	RSNa solution	RSNa loaded PECN
Zero order	**0.9565**	0.8430
First order	0.8909	0.9680
Higuchi	0.9339	**0.9705**
Korsemeyer-Peppas (n)	0.0970 **(0.490)**	0.9594 **(0.521)**

8.21. *Ex vivo* skin permeation study:

The profile of *ex vivo* skin permeation of RSNa solution and RSNa loaded PECN are shown in table- 8.22 and figure- 8.18. In the case of the RSNa solution, over 20.93% of the drug penetrated through the skin in 48 hours. The slow rate of drug permeation could be attributed to the hydrophilic nature of the drug, which resists permeation through the stratum corneum [42, 43]. In case of RSNa loaded PECN, over 58.84 % of RSNa was permeated through skin in 48 hrs, which was higher as compared to RSNa solution might be due to nanosized particles which easily passed through skin layers. The presence of chitosan hydrates the stratum corneum and electrostatically interacts with skin proteins and it reversibly modifies keratin protein structure to create pathway for drug permeation [34, 44, 45]. Chitosan improved skin penetration through trans-appendageal and transcellular pathway [34]. The average flux of RSNa solution and RSNa loaded PECN was found to be 1.28 and 4.65 µg/cm^2/hr respectively, which was 3.63 -folds enhanced as compared to RSNa solution revealed the ability of nanocarriers to enhance skin permeability. The RSNa solution showed more amount of drug remained on skin and minimum retention in skin due to hydrophilic and highly polar nature of drug which hindered to pass through the lipophilic stratum corneum barrier. In case of RSNa loaded

PECN, the more mount of drug retained in the skin and minimum amount of drug remained on the skin as compared to RSNa solution due to nanosize which was easily pass through skin via transcellular pathway. The more retention of RSNa-PECN in the skin was observed due to high positive surface charge which electrostatically interact with negative charged cellular membrane.

Table- 8.22. *Ex vivo* skin permeation profile

Time (In hrs)	**RSNa loaded PECN**	**RSNa Solution**
0	0 ± 0	0 ± 0
1	1.45 ± 0.49	0 ± 0
2	2.23 ± 1.20	0.09 ± 0.04
3	5.67 ± 0.84	0.56 ± 0.25
4	6.41 ± 1.56	1.21 ± 0.63
5	7.34 ± 1.11	2.90 ± 1.02
6	8.84 ± 1.69	2.58 ± 0.87
8	11.59 ± 1.84	3.27 ± 1.26
10	12.94 ± 0.74	5.20 ± 0.98
12	18.56 ± 0.99	7.26 ± 1.58
24	30.27 ± 1.41	9.10 ± 1.36
30	38.48 ± 1.33	15.25 ± 2.01
36	48.82 ± 1.85	16.32 ± 2.24
48	58.84 ± 3.10	20.93 ± 1.52
Parameters	**RSNa loaded PECN**	**Pure RSNa**
Drug remained on skin (%)	19.50 ± 1.01	68.22 ± 4.54
Drug retained in skin (%)	18.60 ± 2.19	10.96 ± 1.79
Transdermal flux (J_{ss}) (µg/cm^2/hr)	4.65	1.28
Steady state flux	4.42	1.63
Permeation enhancement ratio (As compared to pure drug)	3.63	1

(n=3,. ±S.D.)

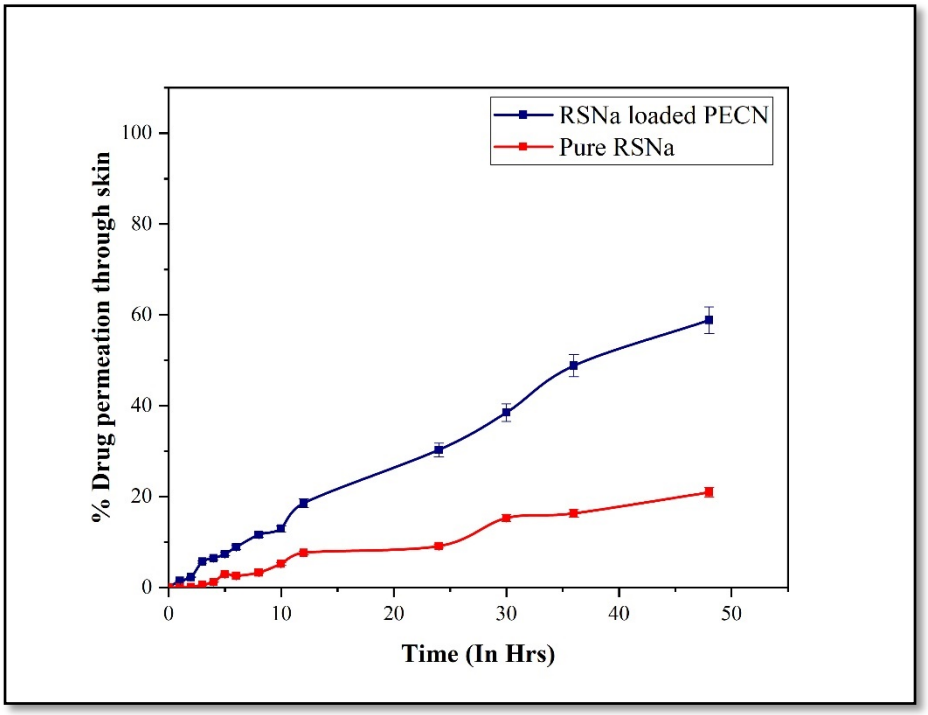

Figure- 8.18. *Ex vivo* skin permeation profile

8.22. In vitro cell viability study:

To evaluate the safety of newly developed PECN, cell viability studies were done on RSNa solution, placebo-PECN, and RSNa-loaded PECN and compared to PBS 7.4 as a positive control and Triton X-100 as a negative control. The results (shown in figure-8.19) showed that there was no significant difference in cell viability after 12 (a) and 24 (b) hours of treatment with placebo PECN and RSNa loaded PECN. The RSNa loaded PECN and placebo PECN showed viability greater than 90 % as compared to RSNa solution treated cell viability (Around 85%) after 24 hrs treatment. The cell viability for PBS 7.4 and triton X-100 was found to be 98.2 and 13.2 % after treatment of 24 hrs. The better cell viability of placebo PECN also revealed that the excipient used in the preparation of PECN is safe for drug delivery through skin. On the basis of results, it was concluded that the novel developed RSNa loaded PECN showed no toxicity to fibroblast cells and it was safe to use in transdermal drug delivery systems.

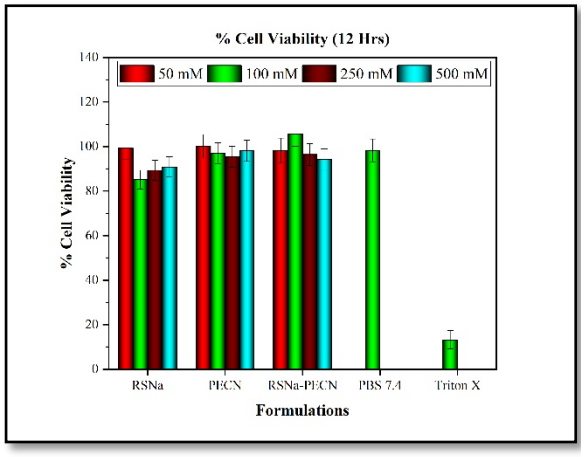

Figure- A. Cell viability at 12 Hrs

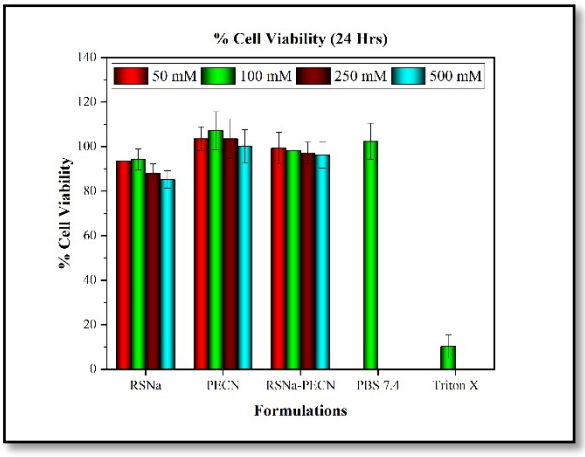

Figure- B. Cell viability at 24 hrs

Figure- 8.19. % Cell viability study

8.23. In vitro cell permeability study:

The results of cell permeability are shown in table- 8.23 and figure- 8.20. The TEER was monitored on 25th day of cell monolayer growth to check integrity of monolayer and it was found to be 910-925 Ωcm2 which was within acceptable range of 500 – 1100 Ωcm2. This TEER value indicated good quality development of cell layers for the transport mechanism [20-22]. Apparent permeability coefficient (Papp) of RSNa loaded PECN was found to be 1.05×10^{-5} cm/s; while, for RSNa solution it was found to be 5.53×10^{-6} cm/s. The permeability coefficient was found to be greater than 1.00×10^{-5} cm/s (considered as higher permeability of substance) [46, 47]. Hence, RSNa loaded PECN had higher permeability capacity through skin layers. RSNa solution permeated over 72.19% drug across cell layers within 12 hours, whilst RSNa loaded PECN permeated over 90% RSNa through cell layer within 10 hours. The results of overall study concluded that the PECN showed more cell permeability due to nanosize of formulation and highly positive surface charge which helped to permeate through cell layers. A positive surface charge nanoparticles favours bioadhesion of the nanoparticles to the negatively-charged cells, thereby facilitating biological interaction with the phospholipid membranes which helps to enhance permeation [48, 49].

Table- 8.23. In vitro cell permeability profile

Time (In Hrs)	RSNa solution	RSNa-PECN
0	0 ± 0	0 ± 0
1	6.27 ± 2.36	9.90 ± 3.63
2	12.12 ± 3.94	18.42 ± 4.15
3	18.35 ± 4.76	32.41 ± 3.48
4	33.88 ± 4.18	46.01 ± 3.25
6	45.56 ± 3.44	66.80 ± 4.10
8	52.57 ± 5.94	78.16 ± 4.86
10	64.40 ± 3.74	93.94 ± 5.48
12	72.19 ± 3.87	
P_{app} (cm/s)	5.53×10^{-6}	1.05×10^{-5}

(n=3, ±S.D.)

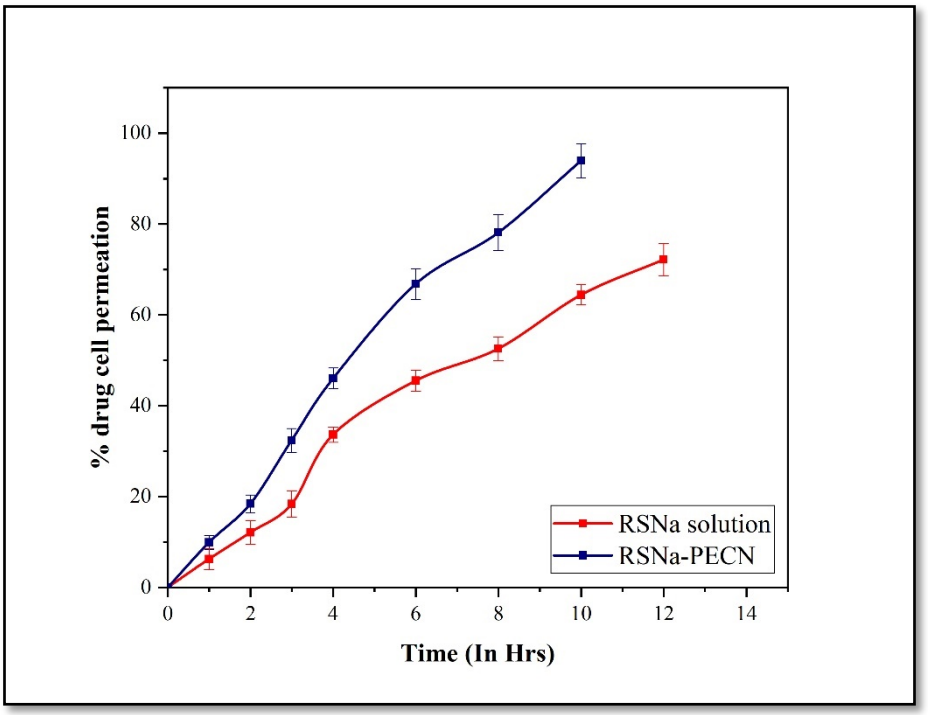

Figure- 8.20. In vitro cell permeability profile

8.24. Stability study:

The results of stability study of RSNa loaded PECN at different storage conditions are represented in table- 8.24 and figure- 8.21. The results showed that no remarkable change was observed in particle size and % assay over 90 days of storage at 2-8 °C and 25±2°C/60 ± 5 % RH. At 40±2°C/75 ± 5 % RH storage condition, there was significant increase in particle size and decrease in % assay was observed over 90 days which might be owing to crystal growth and drug leaching from the polymer matrix caused by elevated temperature conditions [50]. The results of overall study concluded that 2-8 °C and 25±2°C/60 ± 5 % RH were favourable conditions for storing RSNa loaded PECN.

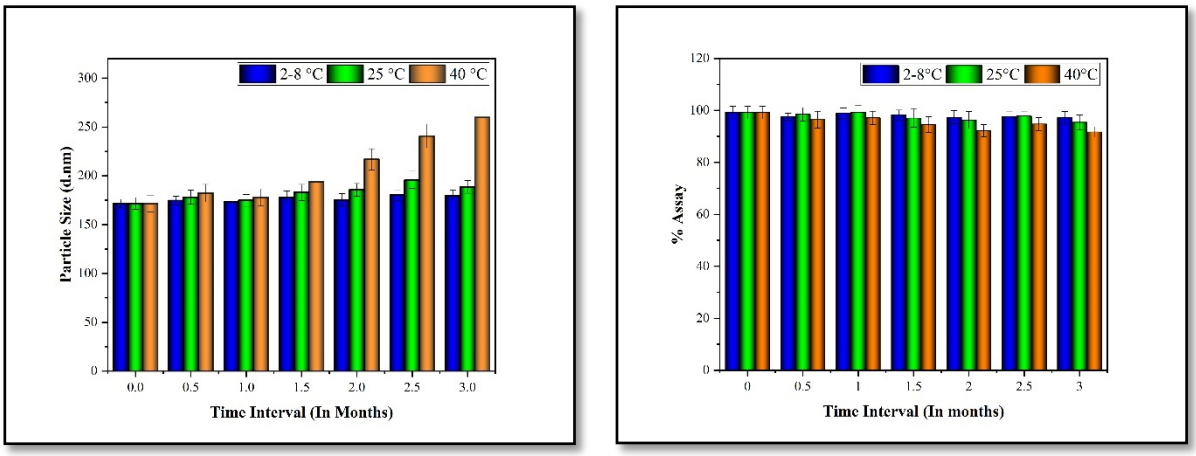

Figure- 8.21. Effect of storage conditions on particle size (a) and % assay (b).

Table- 8.24. Stability study profile

Sr. No.	Time interval (In Month)	Particle Size (d.nm)			% Assay		
		2-8°C	25±2°C/60 ± 5 % RH	40±2°C/75 ± 5 % RH	2-8°C	25±2°C/60 ± 5 % RH	40±2°C/75 ± 5 % RH
1	**Initial**	171.6 ± 4.68	171.6 ± 4.68	171.6 ± 4.68	99.20 ± 2.42	99.20 ± 2.42	99.20 ± 2.42
2	**0.5**	174.6 ± 5.51	178.1 ± 3.71	182.3 ± 5.89	97.61 ± 1.34	98.54 ± 2.68	96.48 ± 3.21
3	**1.0**	173.2 ± 6.32	174.8 ± 4.96	177.9 ± 6.74	98.88 ± 2.01	99.30 ± 2.56	97.12 ± 2.66
4	**1.5**	177.9 ± 4.19	182.9 ± 5.74	193.8 ± 6.09	98.19 ± 2.09	97.10 ± 3.67	94.63 ± 3.04
5	**2.0**	175.3 ± 4.44	185.6 ± 5.96	216.8 ± 8.00	97.36 ± 2.56	96.31 ± 3.31	92.22 ± 2.48
6	**2.5**	180.2 ± 5.17	195.8 ± 5.21	240.7 ± 5.98	97.57 ± 1.90	97.80 ± 1.74	94.78 ± 2.59
7	**3.0**	179.6 ± 5.23	188.6 ± 4.88	259.6 ± 8.91	97.20 ± 2.61	95.44 ± 2.86	91.74 ± 2.01

(n=3, ±S.D.)

Chapter 8 – RSNa loaded PECN

8.25. References:

1. Jardim, K.V., et al., *Physico-chemical characterization and cytotoxicity evaluation of curcumin loaded in chitosan/chondroitin sulfate nanoparticles.* Materials science and engineering: c, 2015. **56**: p. 294-304.
2. Rezazadeh, M., et al., *Incorporation of rosuvastatin-loaded chitosan/chondroitin sulfate nanoparticles into a thermosensitive hydrogel for bone tissue engineering: preparation, characterization, and cellular behavior.* Pharmaceutical Development and Technology, 2019. **24**(3): p. 357-367.
3. Kamani, P., et al., *Phospholipid based ultra-deformable nanovesicular gel for transcutaneous application: QbD based optimization, characterization and pharmacodynamic profiling.* Journal of Drug Delivery Science and Technology, 2019. **51**: p. 152-163.
4. Liang, T., Z. Zhang, and P.J.F.c. Jing, *Black rice anthocyanins embedded in self-assembled chitosan/chondroitin sulfate nanoparticles enhance apoptosis in HCT-116 cells.* Food Chemistry, 2019. **301**: p. 125280.
5. Soe, Z.C., et al., *Folate-targeted nanostructured chitosan/chondroitin sulfate complex carriers for enhanced delivery of bortezomib to colorectal cancer cells.* Asian journal of pharmaceutical sciences, 2019. **14**(1): p. 40-51.
6. Faris, T.M., et al., *Developed simvastatin chitosan nanoparticles co-crosslinked with tripolyphosphate and chondroitin sulfate for ASGPR-mediated targeted HCC delivery with enhanced oral bioavailability.* Saudi Pharmaceutical Journal, 2020. **28**(12): p. 1851-1867.
7. Talib, S., et al., *Chitosan-chondroitin based artemether loaded nanoparticles for transdermal drug delivery system.* Journal of Drug Delivery Science and Technology, 2021. **61**: p. 102281.
8. Abdullah, T.A., N.J. Ibrahim, and M.H. Warsi, *Chondroitin sulfate-chitosan nanoparticles for ocular delivery of bromfenac sodium: Improved permeation, retention, and penetration.* International journal of pharmaceutical investigation, 2016. **6**(2): p. 96.

9. Mahmoud, M.O., et al., *Transdermal delivery of atorvastatin calcium from novel nanovesicular systems using polyethylene glycol fatty acid esters: ameliorated effect without liver toxicity in poloxamer 407-induced hyperlipidemic rats.* Journal of Controlled Release, 2017. **254**: p. 10-22.

10. Aboud, H.M., et al., *Development, optimization, and evaluation of carvedilol-loaded solid lipid nanoparticles for intranasal drug delivery.* AAPS pharmscitech, 2016. **17**(6): p. 1353-1365.

11. Wavikar, P. and P.J.A.p. Vavia, *Nanolipidgel for enhanced skin deposition and improved antifungal activity.* AAPS PharmSciTech, 2013. **14**: p. 222-233.

12. Kim, H., et al., *Characteristics of skin deposition of itraconazole solubilized in cream formulation.* Pharmaceutics, 2019. **11**(4): p. 195.

13. Elshall, A.A., et al., *Ex vivo permeation parameters and skin deposition of melatonin-loaded microemulsion for treatment of alopecia.* Future Journal of Pharmaceutical Sciences volume, 2022. **8**(1): p. 28.

14. Chen, M., X. Liu, and A.J.I.j.o.p. Fahr, *Skin penetration and deposition of carboxyfluorescein and temoporfin from different lipid vesicular systems: In vitro study with finite and infinite dosage application.* International Journal of Pharmaceutics, 2011. **408**(1-2): p. 223-234.

15. Segeritz, C.-P. and L. Vallier, *Cell culture: Growing cells as model systems in vitro*, in *Basic science methods for clinical researchers*. 2017, Elsevier. p. 151-172.

16. Helgason, C.D. and C.L. Miller, *Basic cell culture protocols*. 2005: Totowa, NJ.: Humana Press.

17. Tripathi, B.D. and N. Singh, *Wound Healing Potential of Transdermal Patches Containing Bioactive Fraction: A Novel Approach.* International Journal of Pharmacy & Life Sciences, 2020. **11**(7): p. 83-83.

18. Manca, M.L., et al., *Glycerosomes: Use of hydrogenated soy phosphatidylcholine mixture and its effect on vesicle features and diclofenac skin penetration.* International Journal of Pharmaceutics, 2016. **511**(1): p. 198-204.

19. Manca, M.L., et al., *Glycerosomes: A new tool for effective dermal and transdermal drug delivery.* International Journal of Pharmaceutics, 2013. **455**(1-2): p. 66-74.

20. Shah, P., et al., *In vitro assessment of acyclovir permeation across cell monolayers in the presence of absorption enhancers.* Drug development and industrial pharmacy, 2008. **34**(3): p. 279-288.

21. Chen, S., R. Einspanier, and J. Schoen, *Transepithelial electrical resistance (TEER): a functional parameter to monitor the quality of oviduct epithelial cells cultured on filter supports.* Histochemistry and cell biology, 2015. **144**(5): p. 509-515.

22. Poenar, D.P., et al., *Low-cost method and biochip for measuring the trans-epithelial electrical resistance (TEER) of esophageal epithelium.* Materials, 2020. **13**(10): p. 2354.

23. Sharma, D., et al., *Formulation and optimization of polymeric nanoparticles for intranasal delivery of lorazepam using Box-Behnken design: in vitro and in vivo evaluation.* BioMed research international, 2014. **2014**.

24. Makoni, P.A., K. Wa Kasongo, and R.B. Walker, *Short term stability testing of efavirenz-loaded solid lipid nanoparticle (SLN) and nanostructured lipid carrier (NLC) dispersions.* Pharmaceutics, 2019. **11**(8): p. 397.

25. Al-Nemrawi, N., S. Alsharif, and R.J.I.J.A.P. Dave, *Preparation of chitosan-TPP nanoparticles: the influence of chitosan polymeric properties and formulation variables.* International Journal of Applied Pharmaceutics, 2018. **10**: p. 60-65.

26. Thandapani, G., et al., *Size optimization and in vitro biocompatibility studies of chitosan nanoparticles.* International Journal of Biological Macromolecules, 2017. **104**: p. 1794-1806.

27. Hussain, Z., S.J.I.J.o.P. Sahudin, and P. Sciences, *Preparation, characterisation and colloidal stability of chitosan-tripolyphosphate nanoparticles: optimisation of formulation and process parameters.* International Journal of Pharmacy and Pharmaceutical Sciences 2016. **8**(3): p. 297-308.

28. Chuah, L.H., et al., *Curcumin-containing chitosan nanoparticles as a potential mucoadhesive delivery system to the colon.* Pharm Dev Technol. 2013. **18**(3): p. 591-599.

29. Fàbregas, A., et al., *Impact of physical parameters on particle size and reaction yield when using the ionic gelation method to obtain cationic polymeric chitosan–*

tripolyphosphate nanoparticles. International Journal of Pharmaceutics, 2013. **446**(1-2): p. 199-204.

30. Lee, E.J. and K.-H.J.K.J.o.C.E. Lim, *Polyelectrolyte complexes of chitosan self-assembled with fucoidan: An optimum condition to prepare their nanoparticles and their characteristics.* Korean Journal of Chemical Engineering, 2014. **31**: p. 664-675.

31. Birch, N.P. and J.D.J.L. Schiffman, *Characterization of self-assembled polyelectrolyte complex nanoparticles formed from chitosan and pectin.* Langmuir, 2014. **30**(12): p. 3441-3447.

32. Sangshetti, J.N., et al., *Quality by design approach: Regulatory need.* Arabian Journal of Chemistry, 2017. **10**: p. S3412-S3425.

33. Kumar, A. and M.J.I.j.o.b.m. Ahuja, *Carboxymethyl gum kondagogu–chitosan polyelectrolyte complex nanoparticles: Preparation and characterization.* International Journal of Biological Macromolecules, 2013. **62**: p. 80-84.

34. Gul, R., et al., *Biodegradable ingredient-based emulgel loaded with ketoprofen nanoparticles.* AAPS PharmSciTech, 2018. **19**: p. 1869-1881.

35. Ghumman, S.A., et al., *Chitosan-Linseed mucilage polyelectrolyte complex nanoparticles of Methotrexate: In vitro cytotoxic efficacy and toxicological studies.* Arabian Journal of Chemistry, 2023. **16**(2): p. 104463.

36. Xiong, W., et al., *Auricularia auricular polysaccharide-low molecular weight chitosan polyelectrolyte complex nanoparticles: Preparation and characterization.* Asian Journal of Pharmaceutical Sciences, 2016. **11**(3): p. 439-448.

37. Tan, C., M.J. Selig, and A.J.C.p. Abbaspourrad, *Anthocyanin stabilization by chitosan-chondroitin sulfate polyelectrolyte complexation integrating catechin co-pigmentation.* Carbohydrate Polymers, 2018. **181**: p. 124-131.

38. Joseph, E., G.J.N.f.d.d. Singhvi, and therapy, *Multifunctional nanocrystals for cancer therapy: a potential nanocarrier.* Nanomaterials for Drug Delivery and Therapy, 2019: p. 91-116.

39. Jain, D., et al., *Surface-coated PLA nanoparticles loaded with temozolomide for improved brain deposition and potential treatment of gliomas: development, characterization and in vivo studies.* Drug Delivery, 2016. **23**(3): p. 989-1006.

40. Gul, R., et al., *Biodegradable ingredient-based emulgel loaded with ketoprofen nanoparticles.* AAPS PharmSciTech, 2018. **19**(4): p. 1869-1881.

41. Bruschi, M.L., *Strategies to modify the drug release from pharmaceutical systems*. 2015: Woodhead Publishing.

42. Gyanewali, S., et al., *Formulation development and in vitro–in vivo assessment of protransfersomal gel of anti-resorptive drug in osteoporosis treatment.* International Journal of Pharmaceutics, 2021. **608**: p. 121060.

43. Rawat, P., et al., *Revisiting bone targeting potential of novel hydroxyapatite based surface modified PLGA nanoparticles of risedronate: pharmacokinetic and biochemical assessment.* International Journal of Pharmaceutics, 2016. **506**(1-2): p. 253-261.

44. He, W., et al., *Study on the mechanisms of chitosan and its derivatives used as transdermal penetration enhancers.* international journal of pharmaceutics, 2009. **382**(1-2): p. 234-243.

45. Gul, R., et al., *Functionalised nanostructures for transdermal delivery of drug cargos.* Journal of drug targeting, 2018. **26**(2): p. 110-122.

46. Neupane, R., et al., *Alternatives to biological skin in permeation studies: Current trends and possibilities.* Pharmaceutics, 2020. **12**(2): p. 152.

47. Alvarez-Figueroa, M.J., et al., *Evaluation of the membrane permeability (PAMPA and skin) of benzimidazoles with potential cannabinoid activity and their relation with the Biopharmaceutics Classification System (BCS).* AAPS PharmSciTech., 2011. **12**: p. 573-578.

48. Anitha, A., et al., *Preparation, characterization, in vitro drug release and biological studies of curcumin loaded dextran sulphate–chitosan nanoparticles.* Carbohydrate Polymers, 2011. **84**(3): p. 1158-1164.

49. Jardim, K.V., et al., *Physico-chemical characterization and cytotoxicity evaluation of curcumin loaded in chitosan/chondroitin sulfate nanoparticles.* Drug Delivery, 2015. **56**: p. 294-304.

50. Malviya, R., et al., *Evaluation of Antitumor Efficacy of Chitosan-Tamarind Gum Polysaccharide Polyelectrolyte Complex Stabilized Nanoparticles of Simvastatin.* Int J Nanomedicine, 2021. **16**: p. 2533-2553.